INVITED PAPER

A Mathematical Theory of Network Interference and Its Applications

A unifying framework is developed to characterize the aggregate interference in wireless networks, and several applications are presented.

By Moe Z. Win, *Fellow IEEE*, Pedro C. Pinto, *Student Member IEEE*, and Lawrence A. Shepp

ABSTRACT | In this paper, we introduce a mathematical framework for the characterization of network interference in wireless systems. We consider a network in which the interferers are scattered according to a spatial Poisson process and are operating asynchronously in a wireless environment subject to path loss, shadowing, and multipath fading. We start by determining the statistical distribution of the aggregate network interference. We then investigate four applications of the proposed model: 1) interference in cognitive radio networks; 2) interference in wireless packet networks; 3) spectrum of the aggregate radio-frequency emission of wireless networks; and 4) coexistence between ultrawideband and narrowband systems. Our framework accounts for all the essential physical parameters that affect network interference, such as the wireless propagation effects, the transmission technology, the spatial density of interferers, and the transmitted power of the interferers.

KEYWORDS | Aggregate network interference; coexistence; cognitive radio; emission spectrum; packet networks; spatial Poisson process; stable laws; ultrawideband systems; wireless networks

Manuscript received June 16, 2008; revised October 3, 2008. Current version published March 18, 2009. This work was supported by the Portuguese Science and Technology Foundation under Grant SFRH-BD-17388-2004, the Charles Stark Draper Laboratory Robust Distributed Sensor Networks Program, the Office of Naval Research under Presidential Early Career Award for Scientists and Engineers (PECASE) N00014-09-1-0435, and the National Science Foundation under Grant ANI-0335256.
M. Z. Win and **P. C. Pinto** are with the Laboratory for Information and Decision Systems, Massachusetts Institute of Technology, Cambridge, MA 02139 USA (e-mail: moewin@mit.edu; ppinto@mit.edu).
L. A. Shepp is with the Department of Statistics, Rutgers—The State University, Piscataway, NJ 08854 USA (e-mail: shepp@stat.rutgers.edu).

Digital Object Identifier: 10.1109/JPROC.2008.2008764

I. INTRODUCTION

In a wireless network composed of many spatially scattered nodes, communication is constrained by various impairments such as the *wireless propagation effects*, *network interference*, and *thermal noise*. The effects introduced by propagation in the wireless channel include the attenuation of radiated signals with distance (path loss), the blocking of signals caused by large obstacles (shadowing), and the reception of multiple copies of the same transmitted signal (multipath fading). The network interference is due to accumulation of signals radiated by other transmitters, which undesirably affect receiver nodes in the network. The thermal noise is introduced by the receiver electronics and is usually modeled as additive white Gaussian noise (AWGN).

The modeling of network interference is an important problem, with numerous applications to the analysis and design of communication systems, the development of interference mitigation techniques, and the control of electromagnetic emissions, among many others. In particular, interference modeling has been receiving increased interest in the context of ultrawideband (UWB) technologies, which use extremely large bandwidths and typically operate as an underlay system with other existing narrowband (NB) technologies, such as GSM, GPS, Wi-Fi, and WiMAX. The most common approach is to model the interference by a Gaussian random process [1]–[6]. This is appropriate, for example, when the interference is the accumulation of a large number of independent signals, where no term dominates the sum, and thus the central limit theorem (CLT) applies [7]. The Gaussian process has many well-studied properties and often leads to analytically tractable results. However, there are several scenarios where the CLT does not apply, e.g., when the number of interferers is large but there are

dominant interferers [8]–[11]. In particular, it is known that the CLT gives a very poor approximation for modeling the multiple access interference in time-hopping UWB systems [12], [13]. In many cases, the probability density function (pdf) of the interference exhibits a heavier tail than what is predicted by the Gaussian model. Several mathematical models for impulsive interference have been proposed, including the Class A model [14], [15], the Gaussian-mixture model [16], [17], and the stable model [18], [19].

A model for network interference should capture the essential physical parameters that affect interference, namely: 1) the spatial distribution of the interferers scattered in the network; 2) the transmission characteristics of the interferers, such as modulation, power, and synchronization; and 3) the propagation characteristics of the medium, such as path loss, shadowing, and multipath fading. The spatial location of the interferers can be modeled either deterministically or stochastically. Deterministic models include square, triangular, and hexagonal lattices in the two-dimensional plane [20]–[23], which are applicable when the location of the nodes in the network is exactly known or is constrained to a regular structure. However, in many scenarios, only a statistical description of the location of the nodes is available, and thus a stochastic spatial model is more suitable. In particular, when the terminal positions are unknown to the network designer a priori, we may as well treat them as completely random according to a homogeneous Poisson point process [24].[1] The Poisson process has maximum entropy among all homogeneous processes [25] and corresponds to a simple and useful model for the location of nodes in a network.

The application of the spatial Poisson process to wireless networks has received increased attention in the literature. In the context of the Poisson model, the issues of wireless connectivity and coverage were considered in [26]–[32], while the packet throughput was analyzed in [33]–[38]. The error probability and link capacity in the presence of a Poisson field of interferers were investigated in [39]–[43]. The current literature on network interference is largely constrained to some particular combination of propagation model, spatial location of nodes, transmission technology, or multiple-access scheme; and the existing results are not easily generalizable if some of these system parameters are changed. Furthermore, none of the mentioned studies attempts a unifying characterization that incorporates various metrics, such as outage probability, packet throughput, power spectral density, and error probability.

In this paper, we present a unifying framework for the characterization of network interference. We consider that the interferers are scattered according to a spatial Poisson process and are operating in a wireless environment subject to path loss as well as arbitrary fading and shadowing effects (e.g., Nakagami-*m* fading and log-normal shadowing). The main contributions of the paper are as follows.

- *Distribution of the network interference:* We provide a complete probabilistic characterization of the aggregate network interference generated by the nodes in a wireless network. Our analysis reveals the innate connection between the distribution of the network interference and various important system parameters, such as the path loss exponent, the transmitted power, and the spatial density of the interferers.
- *Interference in cognitive radio networks:* We characterize the statistical distribution of the network interference generated by the secondary users when they are allowed to transmit in the same frequency band of the primary users according to a spectrum-sensing protocol. We analyze the effect of the wireless propagation characteristics on such distribution.
- *Interference in wireless packet networks:* We obtain expressions for the throughput of a link, considering that a packet is successfully received if the signal-to-interference-plus-noise ratio (SINR) exceeds some threshold. We analyze the effect of the propagation characteristics and the packet traffic on the throughput.
- *Spectrum of the aggregate network emission:* We derive the power spectral density (PSD) of the aggregate radio-frequency (RF) emission of a network. Then, we put forth the concept of spectral outage probability (SOP) and present some of its applications, including the establishment of spectral regulations and the design of covert military networks.
- *Coexistence between UWB and NB systems*: We consider a wireless network composed of both UWB and NB nodes. We first determine the statistical distribution of the aggregate UWB interference at any location in the two-dimensional plane. Then, we characterize the error probability of a given NB victim link subject to the aggregate UWB interference.

Our framework accounts for all the essential physical parameters that affect network interference and provides fundamental insights that may be of value to the network designer. In addition, this framework can be applied to various other areas, including noncoherent UWB systems [44], transmitted reference UWB systems [45], and physical-layer security [46].

This paper is organized as follows. Section II describes the system model. Section III derives the representation and distribution of the aggregate interference. Section IV characterizes the interference due to secondary users in cognitive radio networks. Section V analyzes the packet throughput of a link subject to network interference. Section VI characterizes the spectrum of the network interference. Section VII characterizes the error probability of NB communication in the presence of UWB network

[1]The spatial Poisson process is a natural choice in such situations because, given that a node is inside a region $\mathcal{R}$, the pdf of its position is conditionally uniform over $\mathcal{R}$.

interference. Section VIII concludes this paper and summarizes important findings.

II. SYSTEM MODEL

A. Spatial Distribution of the Nodes

We model the spatial distribution of the nodes according to a homogeneous Poisson point process in the two-dimensional infinite plane. The probability of n nodes being inside a region $\mathcal{R}$ (not necessarily connected) depends only on the total area $A_{\mathcal{R}}$ of the region and is given by [24]

$$\mathbb{P}\{n \text{ in } \mathcal{R}\} = \frac{(\lambda A_{\mathcal{R}})^n}{n!} e^{-\lambda A_{\mathcal{R}}}, \quad n \geq 0$$

where λ is the (constant) spatial density of interfering nodes, in nodes per unit area. We define the *interfering nodes* to be the terminals that are transmitting within the frequency band of interest, during the time interval of interest, and hence are effectively contributing to the total interference. Then, irrespective of the network topology (e.g., point-to-point or broadcast) or multiple-access technique (e.g., time or frequency hopping), the above model depends only on the density λ of interfering nodes.[2]

The proposed spatial model is depicted in Fig. 1. For analytical purposes, we assume there is a *probe link* composed of two nodes: the *probe receiver*, located at the origin of the two-dimensional plane (without loss of generality), and the *probe transmitter* (node $i = 0$), deterministically located at a distance r_0 from the origin. All other nodes ($i = 1 \ldots \infty$) are interfering nodes, whose random distances to the origin are denoted by $\{R_i\}_{i=1}^{\infty}$, where $R_1 \leq R_2 \leq \cdots$.

B. Wireless Propagation Characteristics

In many cases of wireless systems design and analysis, it is sufficient to consider the power relationship between the transmitter and receiver to account for the propagation characteristics of the environment. Specifically, we consider that the power P_{rx} received at a distance R from a transmitter is given by

$$P_{\text{rx}} = \frac{P_{\text{tx}} \prod_k Z_k}{R^{2b}} \tag{1}$$

where P_{tx} is the average power measured 1 m away from the transmitter[3]; b is the amplitude loss exponent[4]; and

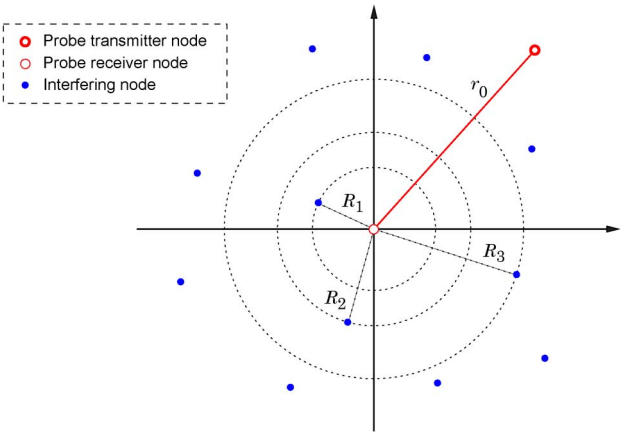

Fig. 1. ***Poisson field model for the spatial distribution of nodes. Without loss of generality, we assume the origin of the coordinate system coincides with the probe receiver.***

$\{Z_k\}$ are independent random variables (RVs), which account for propagation effects such as multipath fading and shadowing. The term $1/R^{2b}$ accounts for the far-field path loss with distance R, where the amplitude loss exponent b is environment-dependent and can approximately range from 0.8 (e.g., hallways inside buildings) to 4 (e.g., dense urban environments), with $b = 1$ corresponding to free-space propagation [48].[5] The proposed model is general enough to account for various propagation scenarios, including the following.

1) *Path loss only*: $Z_1 = 1$.
2) *Path loss and Nakagami-m fading*: $Z_1 = \alpha^2$, where $\alpha^2 \sim \mathcal{G}(m, 1/m)$.[6]
3) *Path loss and log-normal shadowing*: $Z_1 = e^{2\sigma G}$, where $G \sim \mathcal{N}(0,1)$.[7] The term $e^{2\sigma G}$ has a log-normal distribution, where σ is the shadowing coefficient.[8]
4) *Path loss, Nakagami-m fading, and log-normal shadowing*: $Z_1 = \alpha^2$ with $\alpha^2 \sim \mathcal{G}(m, 1/m)$, and $Z_2 = e^{2\sigma G}$ with $G \sim \mathcal{N}(0,1)$.

For cases where the evolution of signals over time is of interest, we consider the waveform relationship between

[2]Time and frequency hopping can be easily accommodated in this model, using the splitting property of Poisson processes [47, Section 6] to obtain the *effective* density of nodes that contribute to the interference.

[3]Unless otherwise stated, we will simply refer to P_{tx} as the "transmitted power."

[4]Note that the *amplitude loss exponent* is b, while the corresponding *power loss exponent* is $2b$.

[5]As we shall see in the rest of this paper, the simple $1/R^{2b}$ dependence allows us to obtain valuable insights in numerous wireless scenarios. However, care must be taken for extremely dense networks, since the close proximity of nodes to the origin would invalidate this far-field dependence.

[6]We use $\mathcal{G}(x, \theta)$ to denote a gamma distribution with mean $x\theta$ and variance $x\theta^2$.

[7]We use $\mathcal{N}(\mu, \sigma^2)$ to denote a Gaussian distribution with mean μ and variance σ^2.

[8]This model for combined path loss and log-normal shadowing can be expressed in logarithmic form [48]–[50], such that the channel loss in decibels is given by $L_{\text{dB}} = k_0 + k_1 \log_{10} r + \sigma_{\text{dB}} G$, where $G \sim \mathcal{N}(0,1)$. The environment-dependent parameters $(k_0, k_1, \sigma_{\text{dB}})$ can be related to (b, σ) as follows: $k_0 = 0$, $k_1 = 20b$, and $\sigma_{\text{dB}} = (20/\ln 10)\sigma$. The parameter σ_{dB} is the standard deviation of the channel loss in dB (or, equivalently, of the received SNR in decibels) and typically ranges from 6 to 12.

the transmitter and receiver in terms of their equivalent low-pass (ELP) representations. Specifically, the ELP received signal can be written as[9]

$$\mathbf{Y}(t) = \frac{\prod_k \sqrt{Z_k}}{R^b} \int \mathbf{h}(t,\tau)\mathbf{X}(t-\tau)d\tau \qquad (2)$$

where the kernel $\mathbf{h}(t,\tau)$ is the time-varying ELP impulse response of the multipath channel, and $\mathbf{X}(t)$ is the ELP transmitted signal. In this case, the RVs $\{Z_k\}$ account for the slow-varying propagation effects (typically, slow-varying log-normal shadowing), while $\mathbf{h}(t,\tau)$ implicitly accounts for the multipath fading. A canonical example for $\mathbf{h}(t,\tau)$ is the tapped-delay line model given by

$$\mathbf{h}(t,\tau) = \sum_q h_q(t) e^{-j2\pi f_c \tau_q(t)} \delta\big(\tau - \tau_q(t)\big) \qquad (3)$$

where f_c is the carrier frequency; $h_q(t)$ and $\tau_q(t)$ are, respectively, the time-varying amplitudes and delays associated with the qth multipath; and $\delta(t)$ denotes the Dirac-delta function.

For the purpose of this paper, the power relation in (1) is sufficient for characterizing interference in cognitive radio networks in Section IV, and for analyzing interference in packet wireless networks in Section V. The time-varying representation in (2) is useful for determining the spectrum of the aggregate network emission in Section VI, and for characterizing coexistence between UWB and NB systems in Section VII.

C. Mobility and Session Lifetime of the Interferers

Typically, the time variation of the distances $\{R_i\}_{i=1}^{\infty}$ of the interferers is highly coupled with that of the shadowing $\{G_i\}_{i=1}^{\infty}$ affecting those nodes. This is because the shadowing is itself associated with the movement of the nodes near large blocking objects. Thus, we introduce the notation $\mathcal{P}$ to succinctly denote "*the distances* $\{R_i\}_{i=1}^{\infty}$ *and shadowing* $\{G_i\}_{i=1}^{\infty}$ *of the interferers*." We consider the distance R_i and the shadowing G_i associated with each interferer to be approximately constant over at least the duration of a symbol, i.e., $R_i(t) \approx R_i$ and $G_i(t) \approx G_i$. Furthermore, we can consider two scenarios that differ in the speed of variation of $\mathcal{P}$ over larger time windows (e.g., the session lifetime of communication).

1) *Slow-varying* $\mathcal{P}$: In this case, the interferers have a long session lifetime during which $\mathcal{P}$ is approximately constant (quasi-static scenario). Thus, it is insightful to *condition* the interference analysis on a given realization of $\mathcal{P}$. As we shall see, this naturally leads to the derivation of *outage metrics* [51]–[54] such as interference outage probability, spectral outage probability, and error outage probability, which in the described scenario are more meaningful than the corresponding $\mathcal{P}$-averaged metrics.
2) *Fast-varying* $\mathcal{P}$: In this case, the interferers have a short session lifetime, where each node periodically becomes active, transmits a burst of symbols, and then turns off (dynamic scenario). Then, the set of interfering nodes (i.e., nodes that are transmitting and contributing to the interference) changes often, and hence $\mathcal{P}$ experiences a variation analogous to that of a fast block fading model. In this scenario, it is insightful to *average* the interference analysis over $\mathcal{P}$, which naturally leads to the derivation of the *average metrics*.

The framework proposed in this paper enables the analysis of both scenarios. In the rest of this paper, we illustrate several applications of our framework for the case of slow-varying $\mathcal{P}$ only. Some examples of the analysis for fast-varying $\mathcal{P}$ can be found in [55] and [56].

III. INTERFERENCE REPRESENTATION AND DISTRIBUTION

In this section, we consider a general model for interference, which will be used to investigate several applications in wireless networks throughout Sections V–VII. Specifically, let $\mathbf{Y} = [Y_1, \ldots, Y_{N_d}]^T$ be a real random vector (RV) of arbitrary dimension N_d, representing the aggregate interference at the probe receiver, located in the origin of the two-dimensional plane (see Fig. 1). For example, the RV $\mathbf{Y}$ can correspond to a projection of the aggregate interference process $Y(t)$ onto some set of basis functions $\{\psi_i(t)\}_{i=1}^{N_d}$. We can express the aggregate interference $\mathbf{Y}$ as

$$\mathbf{Y} = \sum_{i=1}^{\infty} \frac{\mathbf{Q}_i}{R_i^{\eta}} \mathbb{1}_{\mathcal{A}}(\mathbf{Q}_i, R_i) \qquad (4)$$

where

$$\mathbb{1}_{\mathcal{A}}(\mathbf{q}, r) \triangleq \begin{cases} 1, & (\mathbf{q}, r) \in \mathcal{A} \\ 0, & \text{otherwise} \end{cases} \qquad (5)$$

and $\mathbf{Q}_i = [Q_{i,1}, \ldots, Q_{i,N_d}]^T$ represents an arbitrary random quantity associated with interferer i. The purpose of the term $\mathbf{Q}_i$ is to accommodate various propagation effects such as multipath fading and shadowing. The indicator function $\mathbb{1}_{\mathcal{A}}(\mathbf{q}, r)$ allows for the selection of the nodes that contribute to the aggregate interference–the *active users*–based on some condition relating $\mathbf{Q}_i$ and R_i. The proposed model is general

[9]Boldface letters are used to denote complex quantities and vectors.

enough to accommodate various choices of the *active set* $\mathcal{A}$, including the following.

1) If $\mathcal{A} = \{(\mathbf{q}, r) : r \in \mathcal{I}\}$, then (4) represents the aggregate interference resulting from all the nodes inside a region described by $\mathcal{I}$. For example, if $\mathcal{I} = [u, v)$, then (4) represents the aggregate interference resulting from the nodes inside the annulus $u \leq r < v$.
2) If $\mathcal{A} = \{(\mathbf{q}, r) : (|\mathbf{q}|^2/r^{2b}) < P_{\text{th}}\}$, then (4) represents the aggregate interference resulting only from the nodes for which the received power $|\mathbf{Q}_i|^2/R_i^{2b}$ at the origin is below some threshold P_{th}.[10]

The distribution of the aggregate interference $\mathbf{Y}$ plays an important role in the design and analysis of wireless networks, such as in determining the probabilities of interference outage, spectral outage, and error outage.

A. Interference From the Active Set

Theorem 3.1: Let $\{R_i\}_{i=1}^{\infty}$ denote the sequence of distances between the origin and the random points of a two-dimensional Poisson process with spatial density λ. Let $\{\mathbf{Q}_i\}_{i=1}^{\infty}$ be a sequence of N_{d}-dimensional R$\mathbf{V}$s $\mathbf{Q}_i = [Q_{i,1}, \ldots, Q_{i,N_{\text{d}}}]^T$, independent identically distributed (i.i.d.) in i, and independent of the sequence $\{R_i\}$. Let $\mathbf{Y}(\mathcal{A})$ denote the aggregate interference generated by the nodes from the active set $\mathcal{A}$, such that

$$\mathbf{Y}(\mathcal{A}) \triangleq \sum_{i=1}^{\infty} \frac{\mathbf{Q}_i}{R_i^{\eta}} \mathbb{1}_{\mathcal{A}}(\mathbf{Q}_i, R_i)$$

where $\eta > 1$. Then, its characteristic function $\phi_{\mathbf{Y}}(\mathbf{w}, \mathcal{A}) = \mathbb{E}\{e^{j\mathbf{w}\cdot\mathbf{Y}(\mathcal{A})}\}$ is given by

$$\phi_{\mathbf{Y}}(\mathbf{w}, \mathcal{A}) = \exp\left(-2\pi\lambda \int\int \left(1 - e^{\frac{j\mathbf{w}\cdot\mathbf{q}}{r^{\eta}}} \mathbb{1}_{\mathcal{A}}(\mathbf{q}, r)\right) f_{\mathbf{Q}}(\mathbf{q}) d\mathbf{q} r dr\right) \tag{6}$$

where $f_{\mathbf{Q}}(\mathbf{q})$ is the pdf of $\mathbf{Q}_i$.

Proof: This follows immediately from Campbell's theorem [24]. □

Using the above theorem with $\mathcal{A} = \{(\mathbf{q}, r) : r \in \mathcal{I}\}$, we obtain

$$\phi_{\mathbf{Y}}(\mathbf{w}, \mathcal{A}) = \exp\left(-2\pi\lambda \int_{\mathcal{I}} \left[1 - \phi_{\mathbf{Q}}\left(\frac{\mathbf{w}}{r^{\eta}}\right)\right] r dr\right) \tag{7}$$

where $\phi_{\mathbf{Q}}(\mathbf{w})$ is the characteristic function of $\mathbf{Q}_i$. For the case of $\mathcal{A} = \{(\mathbf{q}, r) : (|\mathbf{q}|^2/r^{\eta}) < P^*\}$, we obtain

$$\phi_{\mathbf{Y}}(\mathbf{w}, \mathcal{A}) = \exp\left(-2\pi\lambda \int\int_{\mathcal{Q}} \left(1 - e^{\frac{j\mathbf{w}\cdot\mathbf{q}}{r^{\eta}}}\right) f_{\mathbf{Q}}(\mathbf{q}) d\mathbf{q} r dr\right) \tag{8}$$

where $\mathcal{Q} = \{\mathbf{q} : |\mathbf{q}|^2 < P^* r^{\eta}\}$.

B. Distribution of the Aggregate Interference Amplitude

Using the general result in Section III-A, we now characterize the distribution of the aggregate interference amplitude generated by all the nodes in the plane. The following corollary provides such statistical characterization.

Corollary 3.1 (Symmetric Stable Distribution): Let $\{R_i\}_{i=1}^{\infty}$ denote the sequence of distances between the origin and random points of a two-dimensional Poisson process with spatial density λ. Let $\{\mathbf{Q}_i\}_{i=1}^{\infty}$ be a sequence of spherically symmetric[11] (SS) R$\mathbf{V}$s $\mathbf{Q}_i = [Q_{i,1}, \ldots, Q_{i,N_{\text{d}}}]^T$, i.i.d. in i, independent of the sequence $\{R_i\}$. Let $\mathbf{Y}$ denote the aggregate interference at the origin generated by the nodes scattered in the infinite plane, such that

$$\mathbf{Y} = \sum_{i=1}^{\infty} \frac{\mathbf{Q}_i}{R_i^b}$$

for $b > 1$. Then, its characteristic function $\phi_{\mathbf{Y}}(\mathbf{w}) = \mathbb{E}\{e^{j\mathbf{w}\cdot\mathbf{Y}}\}$ is given by

$$\phi_{\mathbf{Y}}(\mathbf{w}) = \exp(-\gamma|\mathbf{w}|^{\alpha}) \tag{9}$$

where

$$\alpha = \frac{2}{b} \tag{10}$$

$$\gamma = \lambda\pi C_{2/b}^{-1} \mathbb{E}\left\{|Q_{i,n}|^{2/b}\right\} \tag{11}$$

and C_{α} is defined as

$$C_{\alpha} \triangleq \begin{cases} \frac{1-\alpha}{\Gamma(2-\alpha)\cos(\pi\alpha/2)}, & \alpha \neq 1 \\ \frac{2}{\pi}, & \alpha = 1 \end{cases} \tag{12}$$

with $\Gamma(\cdot)$ denoting the gamma function.

[10] As we shall see in Section IV, this is useful for characterizing interference in cognitive radio networks.

[11] A R$\mathbf{V}$ $\mathbf{X}$ is said to be spherically symmetric if its pdf $f_{\mathbf{X}}(\mathbf{x})$ depends only on $|\mathbf{x}|$.

Proof: Using (7) with $\eta = b$, and $\mathcal{I} = [0, \infty)$, we get

$$\phi_{\mathbf{Y}}(\mathbf{w}) = \exp\left(-2\pi\lambda \int_0^\infty \left[1 - \phi_{\mathbf{Q}}\left(\frac{\mathbf{w}}{r^b}\right)\right] r dr\right).$$

If the RV $\mathbf{Q}$ has an SS pdf, its characteristic function is also SS, i.e., $\phi_{\mathbf{Q}}(\mathbf{w}) = \phi_0(|\mathbf{w}|)$ for some $\phi_0(\cdot)$. As a result

$$\phi_{\mathbf{Y}}(\mathbf{w}) = \exp\left(-2\pi\lambda \int_0^\infty \left[1 - \phi_0\left(\left|\frac{\mathbf{w}}{r^b}\right|\right)\right] r dr\right)$$

which, using the change of variable $|\mathbf{w}| r^{-b} = t$, can be rewritten as

$$\phi_{\mathbf{Y}}(\mathbf{w}) = \exp\left(-\pi\lambda |\mathbf{w}|^{2/b} \frac{2}{b} \int_0^\infty \frac{1 - \phi_0(t)}{t^{2/b+1}} dt\right).$$

Appendix I shows that

$$\int_0^\infty \frac{1 - \phi_0(t)}{t^{\alpha+1}} dt = \frac{C_\alpha^{-1}}{\alpha} \mathbb{E}\{|Q_{i,n}|^\alpha\} \tag{13}$$

where C_α is defined in (12), and thus we conclude that the characteristic function of $\mathbf{Y}$ has the simple form given by (9), with parameters α and γ given by (10) and (11), respectively. This completes the proof. □

Random variables with characteristic function of the form of $\phi_{\mathbf{Y}}(\mathbf{w})$ in (9) belong to the class of *symmetric stable RVs*. Stable laws are a direct generalization of Gaussian distributions and include other densities with heavier (algebraic) tails. They share many properties with Gaussian distributions, namely, the stability property and the generalized central limit theorem [7], [57]. Equations (9)–(11) can be succinctly expressed as[12]

$$\mathbf{Y} \sim \mathcal{S}_{N_d}\left(\alpha_{\mathbf{Y}} = \frac{2}{b}, \beta_{\mathbf{Y}} = 0, \gamma_{\mathbf{Y}} = \pi\lambda C_{2/b}^{-1} \mathbb{E}\left\{|Q_{i,n}|^{2/b}\right\}\right) \tag{14}$$

and this notation will be used throughout this paper.

[12]We use $\mathcal{S}(\alpha, \beta, \gamma)$ to denote the distribution of a real stable RV with characteristic exponent $\alpha \in (0, 2]$, skewness $\beta \in [-1, 1]$, and dispersion $\gamma \in [0, \infty)$. The corresponding characteristic function is

$$\phi(w) = \begin{cases} \exp\left(-\gamma|w|^\alpha\left[1 - \jmath\beta\,\mathrm{sign}(w)\tan\left(\frac{\pi\alpha}{2}\right)\right]\right), & \alpha \neq 1 \\ \exp\left(-\gamma|w|\left[1 + \jmath\frac{2}{\pi}\beta\,\mathrm{sign}(w)\ln|w|\right]\right), & \alpha = 1. \end{cases}$$

We use $\mathcal{S}_{N_d}(\alpha, \beta = 0, \gamma)$ to denote the distribution of an N_d-dimensional SS stable $\mathrm{R}\mathbf{V}$ with characteristic exponent α and dispersion γ, and whose characteristic function is $\phi(\mathbf{w}) = \exp(-\gamma|\mathbf{w}|^\alpha)$. Note that each of the N_d individual components of the SS stable $\mathrm{R}\mathbf{V}$ is $\mathcal{S}(\alpha, \beta = 0, \gamma)$.

C. Distribution of the Aggregate Interference Power

In Section III-B, we considered the distribution of the aggregate interference *amplitude*. We now focus on the aggregate interference *power* generated by all the nodes scattered in the plane, where each interferer contributes with the term P_i/R_i^{2b}. The RV P_i represents an arbitrary quantity associated with interferer i and can incorporate various propagation effects such as multipath fading or shadowing, as described in (1). The following corollary provides such statistical characterization.

Corollary 3.2 (Skewed Stable Distribution): Let $\{R_i\}_{i=1}^\infty$ denote the sequence of distances between the origin and the random points of a two-dimensional Poisson process with spatial density λ. Let $\{P_i\}_{i=1}^\infty$ be a sequence of i.i.d. real nonnegative RVs and independent of the sequence $\{R_i\}$. Let I denote the aggregate interference power at the origin generated by all the nodes scattered in the infinite plane, such that

$$I = \sum_{i=1}^\infty \frac{P_i}{R_i^{2b}}$$

for $b > 1$. Then, its characteristic function $\phi_I(w) = \mathbb{E}\{e^{\jmath wI}\}$ is given by

$$\phi_I(w) = \exp\left(-\gamma|w|^\alpha\left[1 - \jmath\beta\,\mathrm{sign}(w)\tan\left(\frac{\pi\alpha}{2}\right)\right]\right) \tag{15}$$

where

$$\alpha = \frac{1}{b} \tag{16}$$

$$\beta = 1 \tag{17}$$

$$\gamma = \pi\lambda C_{1/b}^{-1} \mathbb{E}\left\{P_i^{1/b}\right\} \tag{18}$$

and C_α is defined in (12).

Proof: Using (7) with $N_d = 1$, $\eta = 2b$, $\mathcal{I} = [0, \infty)$, we get

$$\phi_I(w) = \exp\left(-2\pi\lambda \int_0^\infty \left[1 - \phi_P\left(\frac{w}{r^{2b}}\right)\right] r dr\right)$$

where $\phi_P(w)$ is the characteristic function of P_i. Using the change of variable $|w| r^{-2b} = t$, this can be rewritten as

$$\phi_I(w) = \exp\left(-\pi\lambda |w|^{1/b} \frac{1}{b} \int_0^\infty \frac{1 - \mathbb{E}\left\{e^{\jmath\,\mathrm{sign}(w) P_i t}\right\}}{t^{1/b+1}} dt\right).$$

Appendix II shows that

$$\int_0^\infty \frac{1-\mathbb{E}\left\{e^{\jmath\,\mathrm{sign}(w)P_i t}\right\}}{t^{\alpha+1}}dt = \mathbb{E}\left\{P_i^\alpha\right\}\frac{C_\alpha^{-1}}{\alpha}\left[1-\jmath\,\mathrm{sign}(w)\tan\left(\frac{\pi\alpha}{2}\right)\right] \quad (19)$$

where C_α is defined in (12), and thus we conclude that the characteristic function of I has the simple form given by (15), with parameters α, β, and γ given by (16)–(18). This completes the proof. □

Random variables with characteristic function of the form $\phi_I(w)$ in (15) belong to the class of *skewed stable RVs*. Using the notation introduced before, (15)–(18) can be succinctly expressed as

$$I \sim \mathcal{S}\left(\alpha=\frac{1}{b},\beta=1,\gamma=\pi\lambda C_{1/b}^{-1}\mathbb{E}\left\{P_i^{1/b}\right\}\right). \quad (20)$$

In the remainder of this paper, we will show how the theory developed in this section is useful to characterize interference in wireless networks, enabling a wide variety of applications.

IV. INTERFERENCE IN COGNITIVE RADIO NETWORKS

With the increasing need for higher data rates, the electromagnetic spectrum has become a scarce resource. Such shortage is in part due to the current allocation policies, which allocate spectral bands for exclusive use of a single entity within a geographical area. Studies show that the licensed spectrum is mostly underused across time and geographical regions [58]. One solution that enables a more efficient use of the spectrum is *cognitive radio*, a new paradigm in which a wireless terminal—the *secondary user*—can dynamically access unused licensed spectrum, while avoiding interference with its owner—the *primary user* [59]. One example of such cognitive behavior is spectrum sensing, i.e., the ability to actively monitor the occupation of spectrum bands. It is of critical importance to develop models for cognitive radio networks, which not only quantify their communication performance but also provide guidelines for the design of practical cognitive algorithms.

In this section, we consider an application of the proposed framework to the characterization and control of the aggregate interference in cognitive radio networks. Specifically, we wish to quantify the performance of the primary users, when the secondary users are allowed to transmit in the same band, according to a spectrum-sensing protocol. We consider the spatial model depicted in Fig. 1, where a primary link operates in the presence of secondary users, which are scattered in the plane according to an homogeneous Poisson process $\breve{\Pi}_{\mathrm{sec}}$, with density λ_{sec}. When a primary transmission occurs, the handshake procedure between the primary transmitter and receiver would trigger the *primary receiver* to transmit a beacon with power P_{pri}, thus indicating its presence to the secondary nodes. When a secondary user senses such beacon, it is not allowed to transmit, in order to reduce interference caused to the primary link. However, due to the wireless propagation effects such as multipath fading and shadowing, the secondary users may miss detecting this beacon, and may still transmit and interfere with the primary link. The probability $p_{\mathrm{d}}(r)$ that a secondary user detects the beacon transmitted by the primary receiver at a distance r is given by

$$p_{\mathrm{d}}(r) = \mathbb{P}_{\{Z_k\}}\left\{\frac{P_{\mathrm{pri}}\prod_k Z_k}{r^{2b}} \geq P^*\right\} \quad (21)$$

where P_{pri} is the average transmit power of the beacon; P^* denotes the threshold for beacon detection (e.g., related to the detection sensitivity of the secondary users); and the other parameters have the same meaning as in (1).

In what follows, we characterize the distribution of the network interference generated by all the secondary nodes that are not able to detect the primary beacon, and thus contribute to a performance degradation of the primary link.

A. Distribution of the Network Interference Due to Secondary Users

The power I_{sec} of the network interference generated by the secondary nodes can be written as

$$I_{\mathrm{sec}} \triangleq \sum_{i=1}^{\infty}\frac{P_{\mathrm{sec}}Z_i}{R_i^{2b}}\mathbb{1}_{\mathcal{A}}(\mathbf{q},r)$$

where $Z_i \triangleq \prod_k Z_{i,k}$ accounts for the random propagation effects associated with node i and

$$\mathcal{A} = \left\{(z,r) : \frac{P_{\mathrm{pri}}z}{r^{2b}} < P^*\right\}.$$

Using (8) with $N_{\mathrm{d}}=1$, $\eta=2b$, and $\mathbf{Q}=P_{\mathrm{sec}}Z$, we can write

$$\phi_{I_{\mathrm{sec}}}(w) = \exp\left(-2\pi\lambda_{\mathrm{sec}}\int_0^\infty\int_0^{\frac{P^*r^{2b}}{P_{\mathrm{pri}}}}\left(1-e^{\frac{\jmath wP_{\mathrm{sec}}z}{r^{2b}}}\right)f_Z(z)rdzdr\right) \quad (22)$$

where $f_Z(z)$ is the pdf of Z_i. Alternatively, we can obtain an equivalent expression for (22) by changing the order of integration as

$$\phi_{I_{\text{sec}}}(w) = \exp\left(-2\pi\lambda_{\text{sec}} \int_0^{\infty}\int_{\left(\frac{P_{\text{pri}}z}{P^*}\right)^{1/2b}}^{\infty}\left(1-e^{\frac{\eta w P_{\text{sec}} z^2}{r^{2b}}}\right) f_Z(z) r dr dz\right).$$

Although in general $\phi_{I_{\text{sec}}}(w)$ cannot be determined in closed form, it can be used to numerically evaluate [60], [61] various performance metrics of interest, such as the *interference outage probability*, given by

$$P_{\text{out}} = \mathbb{P}\{I_{\text{sec}} > I^*\} = 1 - F_{I_{\text{sec}}}(I^*)$$

where $F_{I_{\text{sec}}}(\cdot)$ is the cumulative distribution function (cdf) of the RV I_{sec}.

B. Effect of the Propagation Characteristics on p_{d}

The ability of a secondary user to detect the primary beacon is essential in controlling the interference generated to the primary link. Therefore, it is important to understand the behavior of the detection probability p_{d} for various propagation conditions, including the four different scenarios described in Section II-B.

1) *Path loss only:* In this case, a secondary node can detect the primary beacon if it is located inside a circle of radius $(P_{\text{pri}}/P^*)^{1/2b}$ around the primary receiver, also known as the *exclusion* or *no-talk radius*. Thus, (21) reduces to

$$p_{\text{d}}(r) = \begin{cases} 1, & 0 \le r \le \left(\frac{P_{\text{pri}}}{P^*}\right)^{\frac{1}{2b}} \\ 0, & \text{otherwise.} \end{cases}$$

2) *Path loss and Nakagami-m fading:* In this case, (21) reduces to $p_{\text{d}}(r) = \mathbb{P}_{\alpha}\{\alpha^2 \ge P^* r^{2b}/P_{\text{pri}}\}$, where $\alpha^2 \sim \mathcal{G}(m, 1/m)$. Using the cdf of a gamma RV, we obtain

$$p_{\text{d}}(r) = 1 - \frac{1}{\Gamma(m)}\gamma_{\text{inc}}\left(m, \frac{P^* r^{2b} m}{P_{\text{pri}}}\right) \qquad (23)$$

where $\gamma_{\text{inc}}(a,x) = \int_0^x t^{a-1}e^{-t}dt$ is the lower incomplete gamma function. For integer m, we can express $\gamma_{\text{inc}}(a,x)$ in closed form [62], so that (23) simplifies to

$$p_{\text{d}}(r) = 1 - \frac{(m-1)!}{\Gamma(m)}\left(1 - \sum_{k=0}^{m-1}\frac{\nu_1^k e^{-\nu_1}}{k!}\right)$$

where

$$\nu_1 = \frac{P^* r^{2b} m}{P_{\text{pri}}}.$$

For the particular case of Rayleigh fading ($m = 1$), we obtain

$$p_{\text{d}}(r) = \exp\left(-\frac{P^* r^{2b}}{P_{\text{pri}}}\right).$$

3) *Path loss and log-normal shadowing:* In this case, (21) reduces to $p_{\text{d}}(r) = \mathbb{P}_G\{e^{2\sigma G} \ge P^* r^{2b}/P_{\text{pri}}\}$, where $G \sim \mathcal{N}(0,1)$. Using the Gaussian Q-function, we obtain

$$p_{\text{d}}(r) = Q\left(\frac{1}{2\sigma}\ln\left(\frac{P^* r^{2b}}{P_{\text{pri}}}\right)\right).$$

4) *Path loss, Nakagami-m fading, and log-normal shadowing:* In this case, (21) reduces to $p_{\text{d}}(r) = \mathbb{P}_{\alpha,G}\{\alpha^2 e^{2\sigma G} \ge P^* r^{2b}/P_{\text{pri}}\}$. Conditioning on G, using the cdf of a gamma RV, and then averaging over G, we obtain

$$p_{\text{d}}(r) = 1 - \frac{1}{\Gamma(m)}\mathbb{E}_G\left\{\gamma_{\text{inc}}\left(m, \frac{P^* r^{2b} m}{P_{\text{pri}} e^{2\sigma G}}\right)\right\}.$$

In [63], we show that if we consider m to be an integer and also approximate the moment generating function of the log-normal RV $e^{-2\sigma G}$ by a Gauss–Hermite series, $p_{\text{d}}(r)$ simplifies to

$$p_{\text{d}}(r) \approx 1 - \frac{(m-1)!}{\Gamma(m)}\left(1 - \frac{1}{\sqrt{\pi}}\sum_{k=0}^{m-1}\sum_{n=1}^{N_{\text{p}}} H_{x_n}\frac{\nu_2^k e^{-\nu_2}}{k!}\right) \qquad (24)$$

where

$$\nu_2 = \frac{P^* r^{2b} m}{P_{\text{pri}}} e^{2\sqrt{2}\sigma x_n}$$

and x_n and H_{x_n} are, respectively, the zeros and the weights of the N_{p}-order Hermite polynomial. Both x_n and H_{x_n} are tabulated in [62, Table 25.10] for various polynomial orders N_{p}. Typically, setting $N_{\text{p}} = 12$ ensures that the approximation

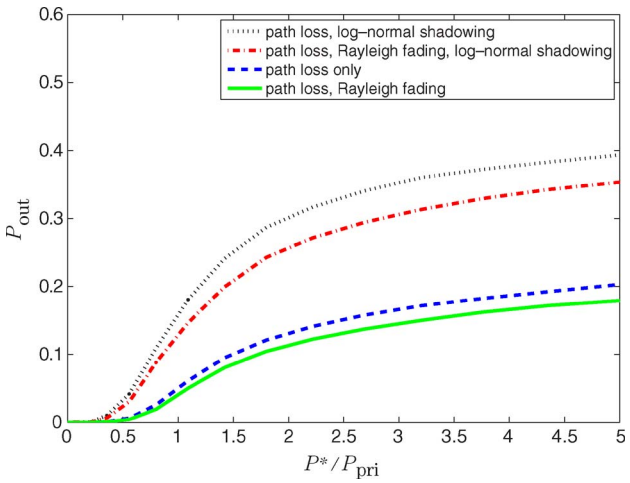

Fig. 2. *Interference outage probability P_{out} versus the normalized detection threshold P^*/P_{pri} for various wireless propagation characteristics ($I^*/P_{\text{sec}} = 1$, $\lambda_{\text{sec}} = 0.1\ \text{m}^{-2}$, $b = 2$, $\sigma_{\text{dB}} = 10$).*

in (24) is extremely accurate [64]. For the particular case of Rayleigh fading ($m = 1$), (24) simplifies to

$$p_{\text{d}}(r) \approx \frac{1}{\sqrt{\pi}} \sum_{n=1}^{N_{\text{p}}} H_{x_n} \exp\left(-\frac{P^* r^{2b}}{P_{\text{pri}}} e^{2\sqrt{2}\sigma x_n}\right).$$

C. Numerical Results

Fig. 2 illustrates the dependence of the interference outage probability P_{out} on the beacon detection threshold P^* for various wireless propagation characteristics. Note that both the multipath fading and shadowing have two opposing effects in P_{out}: on one hand, if a secondary user experiences a severely faded channel, then it misses the primary beacon detection and still transmits, thus *increasing* the P_{out} of the primary link; on the other hand, due to the reciprocity of the wireless channel, the interference contribution of such secondary user will be severely attenuated, thus *decreasing* P_{out}. Fig. 2 shows that, for the considered example, when compared to the case in which only path loss is present, the Rayleigh fading improves the performance of the primary link, while the log-normal shadowing degrades such performance.

V. INTERFERENCE IN WIRELESS PACKET NETWORKS

A wireless network is typically composed of many spatially scattered nodes, which compete for shared network resources, such as the electromagnetic spectrum. A traditional measure of how much traffic can be delivered by such a network is the packet throughput. In a wireless environment, the throughput is constrained by various impairments that affect communication between nodes, such as wireless propagation effects, network interference, and thermal noise. Here we develop a framework that quantifies the impact of all these impairments on the packet throughput, incorporating other important network parameters, such as the spatial distribution of nodes and their transmission characteristics [63], [65].

The proposed spatial model is depicted in Fig. 1. Our goal is to determine the throughput of the probe link subject to the effect of all the interfering nodes in the network. We consider that the power P_{rx} received at a distance R from a transmitter is given by (1) and carry out the analysis in terms of general propagation effects $\{Z_k\}$. Interfering nodes are considered to have the same transmit power P_{I}—a plausible constraint when power control is too complex to implement, for example, in decentralized ad hoc networks. For generality, however, we allow the probe node to employ an arbitrary power P_0, not necessarily equal to that of the interfering nodes.

We analyze the case of half-duplex transmission, where each device transmits and receives at different time intervals, since full-duplexing capabilities are rare in typical low-cost applications. Nevertheless, the results presented in this paper can be easily modified to account for the full-duplex case. We further consider the scenario where all nodes transmit with the same traffic pattern. In particular, we examine three types of traffic, as depicted in Fig. 3.

1) *Slotted-synchronous traffic:* Similar to the slotted ALOHA protocol [66], the nodes are synchronized and transmit in slots of duration L_{p}

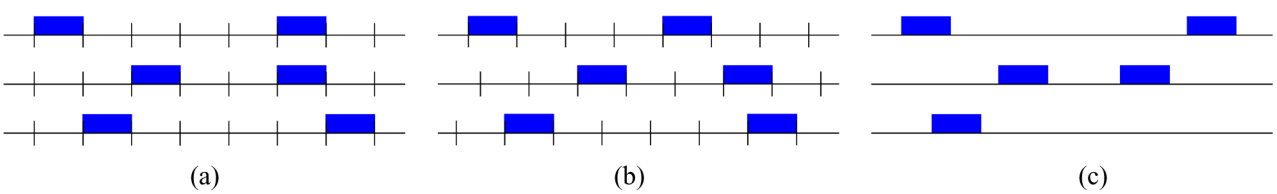

Fig. 3. *Three types of packet traffic, as observed by the node at the origin. (a) Slotted-synchronous transmission. (b) Slotted-asynchronous transmission. (c) Exponential-interarrival transmission.*

seconds.[13] A node transmits in a given slot with probability q. The transmissions are independent for different slots and for different nodes.

2) *Slotted-asynchronous traffic:* The nodes transmit in slots of duration L_p seconds, which are not synchronized with other nodes' time slots. A node transmits in a given slot with probability q. The transmissions are independent for different slots or for different nodes.
3) *Exponential-interarrivals traffic:* The nodes transmit packets of duration L_p seconds. The idle time between packets is exponentially distributed with mean $1/\lambda_p$.[14]

In what follows, we analyze the throughput of the probe link from an SINR perspective. In such approach, a node can hear the transmissions from *all* the nodes in the two-dimensional plane.[15] A packet is successfully received if the SINR exceeds some threshold. Therefore, we start with the statistical characterization of the SINR and then use those results to analyze the throughput.

A. Signal-to-Interference-Plus-Noise Ratio

Typically, the distances $\{R_i\}$ and propagation effects $\{Z_{i,k}\}$ associated with node i are slowly varying and remain approximately constant during the packet duration L_p. In this quasi-static scenario, it is insightful to define the SINR conditioned on a given realization of those RVs. As we shall see, this naturally leads to the derivation of an *SINR outage probability*, which in turn determines the throughput. We start by formally defining the SINR.

Definition 5.1 (SINR): The SINR associated with the node at the origin is defined as

$$\mathrm{SINR} \triangleq \frac{S}{I+N} \tag{25}$$

where S is the power of the desired signal received from the probe node, I is the aggregate interference power received from all other nodes in the network, and N is the (constant) noise power. Both S and I depend on a given realization of $\{R_i\}$, $i = 1 \ldots \infty$, and $\{Z_{i,k}\}$, $i = 0 \ldots \infty$.

[13]By convention, we define these types of traffic with respect to the receiver clock. In the typical case where the propagation delays with respect to the packet length can be ignored, all nodes in the plane observe exactly the same packet arrival process.

[14]This is equivalent to each node using a $M/D/1/1$ queue for packet transmission, characterized by a Poisson arrival process with rate λ_p, a constant service time L_p, a single server, and a buffer of one packet.

[15]This contrasts with a connectivity-based framework [63], where a node can only hear the transmissions from a finite number of nodes (called *audible interferers*) whose received power exceeds some threshold. In such approach, for a node to successfully receive the desired packet, it must not collide with any other packet from the audible interferers.

Using (1), the desired signal power S can be written as

$$S = \frac{P_0 \prod_k Z_{0,k}}{r_0^{2b}} \tag{26}$$

where the subscript 0 refers to the probe link. Similarly, the aggregate interference power I can be written as

$$I = \sum_{i=1}^{\infty} \frac{P_I \Delta_i \prod_k Z_{i,k}}{R_i^{2b}} \tag{27}$$

where P_I is the transmitted power associated with each interferer and $\Delta_i \in [0,1]$ is the (random) duty-cycle factor associated with interferer i. As we shall see, the RV Δ_i accounts for the different traffic patterns of nodes and is equal to the fraction of the duration L_p during which interferer i is effectively transmitting. Note that since S and I depend on the random node positions and random propagation effects, they can be seen as RVs whose value is different for each realization of those random quantities. The distribution of the RV I can be determined from Corollary 3.2, setting $P_i = P_I \Delta_i \prod_k Z_{i,k}$. Then, it follows that I has a skewed stable distribution given by

$$I \sim \mathcal{S}\left(\alpha = \frac{1}{b}, \beta = 1, \gamma = \pi \lambda C_{1/b}^{-1} P_I^{1/b} \mathbb{E}\left\{\Delta_i^{1/b}\right\} \prod_k \mathbb{E}\left\{Z_{i,k}^{1/b}\right\}\right) \tag{28}$$

where $b > 1$ and C_α is defined in (12). As we shall see, the probe link throughput depends on the traffic pattern of the nodes only through $\mathbb{E}\{\Delta_i^{1/b}\}$ in (28).

B. Probe Link Throughput

We now use the results developed in Section V-A to characterize the throughput of the probe link, subject to the aggregate network interference. We start by defining the concept of throughput.

Definition 5.2: The *throughput* $\mathcal{T}$ of a link is the probability that a packet is successfully received during an interval equal to the packet duration L_p. For a packet to be successfully received, the SINR of the link must exceed some threshold.

Using the definition above, we can write the throughput $\mathcal{T}$ as

$$\mathcal{T} = \mathbb{P}\{\text{probe transmits}\}\mathbb{P}\{\text{receiver silent}\}\mathbb{P}\{\text{no outage}\}. \tag{29}$$

The first probability term, which we denote by p_{T}, depends on the type of packet traffic. The second term, which we denote by p_{S}, also depends on the type of packet traffic and corresponds to the probability that the node at the origin is silent (i.e., does not transmit) during the transmission of the packet by the probe node. This second term is necessary because the nodes are half-duplex, so they cannot transmit and receive simultaneously. The third term is simply $\mathbb{P}\{\mathsf{SINR} \geq \theta^*\}$, where θ^* is a predetermined threshold that ensures reliable packet communication over the probe link. Therefore, the throughput of a wireless packet network can be written as

$$\mathcal{T} = p_{\mathrm{T}} p_{\mathrm{S}} \mathbb{P}\{\mathsf{SINR} \geq \theta^*\}. \tag{30}$$

Using (25), (26), and the law of total probability with respect to RVs $\{Z_{0,k}\}$ and I, we can write

$$\mathbb{P}\{\mathsf{SINR} \geq \theta^*\} = \mathbb{E}_I\left\{\mathbb{P}_{\{Z_{0,k}\}}\left\{\prod_k Z_{0,k} \geq \frac{r_0^{2b}\theta^*}{P_0}(I+N)\middle| I\right\}\right\} \tag{31}$$

or, alternatively

$$\mathbb{P}\{\mathsf{SINR} \geq \theta^*\} = \mathbb{E}_{\{Z_{0,k}\}}\left\{F_I\left(\frac{P_0\prod_k Z_{0,k}}{r_0^{2b}\theta^*} - N\right)\right\} \tag{32}$$

where $F_I(\cdot)$ is the cdf of the stable RV I, whose distribution is given in (28). As we shall see, both forms are useful depending on the considered propagation characteristics. Equations (30)–(32) are general and valid for a variety of propagation conditions as well as traffic patterns. As we will see in the next sections, the propagation characteristics determine only $\mathbb{P}\{\mathsf{SINR} \geq \theta^*\}$, while the traffic pattern determines p_{T}, p_{S}, and $\mathbb{P}\{\mathsf{SINR} \geq \theta^*\}$.

C. Effect of the Propagation Characteristics on $\mathcal{T}$

We now determine the effect of four different propagation scenarios described in Section II-B on the throughput. Recall that the propagation characteristics affect the throughput $\mathcal{T}$ only through $\mathbb{P}\{\mathsf{SINR} \geq \theta^*\}$ in (30), and so we now derive such probability for these specific scenarios.

1) *Path loss only:* In this case, the expectation in (32) disappears and we have

$$\mathbb{P}\{\mathsf{SINR} \geq \theta^*\} = F_I\left(\frac{P_0}{r_0^{2b}\theta^*} - N\right) \tag{33}$$

where the distribution of I in (28) reduces to

$$I \sim \mathcal{S}\left(\alpha = \frac{1}{b}, \beta = 1, \gamma = \pi\lambda C_{1/b}^{-1} P_{\mathrm{I}}^{1/b} \mathbb{E}\left\{\Delta_i^{1/b}\right\}\right).$$

Note that the characteristic function of I was also obtained in [35] using the influence function method, for the case of path loss and slotted-synchronous traffic only.

2) *Path loss and Nakagami-m fading:* In this case, (31) reduces to

$$\mathbb{P}\{\mathsf{SINR} \geq \theta^*\} = 1 - \frac{1}{\Gamma(m)}\mathbb{E}_I\left\{\gamma_{\mathrm{inc}}\left(m, \frac{r_0^{2b}\theta^*(I+N)m}{P_0}\right)\right\}.$$

For integer m, this can be expressed in closed form [63] as

$$\mathbb{P}\{\mathsf{SINR} \geq \theta^*\} = 1 - \frac{(m-1)!}{\Gamma(m)}\left(1 - \sum_{k=0}^{m-1}\sum_{j=0}^{k}\frac{(-\nu_3)^j}{j!} \times \frac{(\nu_3 N)^{k-j}e^{-\nu_3 N}}{(k-j)!}\frac{d^j\phi_I(s)}{ds^j}\bigg|_{s=\nu_3}\right) \tag{34}$$

where

$$\nu_3 = \frac{r_0^{2b}\theta^* m}{P_0}$$

and

$$\phi_I(s) = \exp\left(-\frac{\pi\lambda C_{1/b}^{-1} P_{\mathrm{I}}^{1/b}\Gamma\left(m+\frac{1}{b}\right)\mathbb{E}\left\{\Delta_i^{1/b}\right\}}{m^{1/b}\Gamma(m)\cos\left(\frac{\pi}{2b}\right)}s^{1/b}\right)$$

for $s \geq 0$. For the particular case of Rayleigh fading ($m = 1$), we obtain

$$\mathbb{P}\{\mathsf{SINR} \geq \theta^*\} = \exp\left(-\frac{r_0^{2b}\theta^* N}{P_0}\right) \times \exp\left[-\frac{\pi\lambda C_{1/b}^{-1}\Gamma\left(1+\frac{1}{b}\right)\mathbb{E}\left\{\Delta_i^{1/b}\right\}}{\cos\left(\frac{\pi}{2b}\right)}\left(\frac{P_{\mathrm{I}} r_0^{2b}\theta^*}{P_0}\right)^{1/b}\right]. \tag{35}$$

3) *Path loss and log-normal shadowing:* In this case, (31) reduces to

$$\mathbb{P}\{\mathsf{SINR} \geq \theta^*\} = \mathbb{E}_I\left\{Q\left(\frac{1}{2\sigma}\ln\left[\frac{r_0^{2b}\theta^*(I+N)}{P_0}\right]\right)\right\} \quad (36)$$

where $Q(\cdot)$ denotes the Gaussian Q-function, and the distribution of I in (28) reduces to

$$I \sim \mathcal{S}\left(\alpha = \frac{1}{b}, \beta = 1, \gamma = \pi\lambda C_{1/b}^{-1} P_{\mathrm{I}}^{1/b} e^{2\sigma^2/b^2}\mathbb{E}\left\{\Delta_i^{1/b}\right\}\right).$$

4) *Path loss, Nakagami-m fading, and log-normal shadowing*: In this case, (31) reduces to

$$\mathbb{P}\{\mathsf{SINR} \geq \theta^*\} = 1 - \frac{1}{\Gamma(m)} \times \mathbb{E}_{G_0,I}\left\{\gamma_{\mathrm{inc}}\left(m, \frac{r_0^{2b}\theta^*(I+N)m}{P_0 e^{2\sigma G_0}}\right)\right\} \quad (37)$$

where the distribution of I in (28) reduces to

$$I \sim \mathcal{S}\left(\alpha = \frac{1}{b}, \beta = 1, \gamma = \pi\lambda C_{1/b}^{-1} P_{\mathrm{I}}^{1/b} e^{2\sigma^2/b^2}\mathbb{E}\left\{\Delta_i^{1/b}\right\}\frac{\Gamma\left(m+\frac{1}{b}\right)}{m^{1/b}\Gamma(m)}\right).$$

For integer m, this can be expressed in closed form [63] as

$$\mathbb{P}\{\mathsf{SINR} \geq \theta^*\} = 1 - \frac{(m-1)!}{\Gamma(m)} \times \left(1 - \sum_{k=0}^{m-1}\sum_{j=0}^{k}\mathbb{E}_{G_0}\left\{\frac{(-\nu_4)^j}{j!}\frac{(\nu_4 N)^{k-j}e^{-\nu_4 N}}{(k-j)!}\frac{d^j\phi_I(s)}{ds^j}\bigg|_{s=\nu_4}\right\}\right) \quad (38)$$

where

$$\nu_4 = \frac{r_0^{2b}\theta^* m}{P_0 e^{2\sigma G_0}}$$

and

$$\phi_I(s) = \exp\left(-\frac{\pi\lambda C_{1/b}^{-1} P_{\mathrm{I}}^{1/b} e^{2\sigma^2/b^2}\Gamma\left(m+\frac{1}{b}\right)\mathbb{E}\left\{\Delta_i^{1/b}\right\}}{m^{1/b}\Gamma(m)\cos\left(\frac{\pi}{2b}\right)}s^{1/b}\right)$$

for $s \geq 0$. For the particular case of Rayleigh fading ($m = 1$), we obtain

$$\mathbb{P}\{\mathsf{SINR} \geq \theta^*\} = \mathbb{E}_{G_0}\left\{\exp\left(-\frac{r_0^{2b}\theta^* N}{P_0 e^{2\sigma G_0}}\right)\left(-\frac{\pi\lambda C_{1/b}^{-1} e^{2\sigma^2/b^2}\Gamma\left(1+\frac{1}{b}\right)\mathbb{E}\left\{\Delta_i^{1/b}\right\}}{\cos\left(\frac{\pi}{2b}\right)} \times \left(\frac{P_{\mathrm{I}} r_0^{2b}\theta^*}{P_0 e^{2\sigma G_0}}\right)^{1/b}\right)\right\}. \quad (39)$$

D. Effect of the Traffic Pattern on $\mathcal{T}$

We now investigate the effect of three different types of traffic pattern on the throughput. Recall that the traffic pattern affects the throughput $\mathcal{T}$ through p_{T}, p_{S}, and $\mathbb{P}\{\mathsf{SINR} \geq \theta^*\}$ in (30). The type of packet traffic determines the statistics of the duty-cycle factor Δ_i, and in particular $\mathbb{E}\{\Delta_i^{1/b}\}$ in (28), which in turn affects $\mathbb{P}\{\mathsf{SINR} \geq \theta^*\}$.

1) *Slotted-synchronous traffic:* In this case, $p_{\mathrm{T}} = q$ and $p_{\mathrm{S}} = 1 - q$. The duty-cycle factor Δ_i is a binary RV taking the value zero or one, and we can show [63] that $\mathbb{E}\{\Delta_i^{1/b}\} = q$.
2) *Slotted-asynchronous traffic:* In this case, $p_{\mathrm{T}} = q$ and $p_{\mathrm{S}} = (1-q)^2$. The duty-cycle factor Δ_i is zero, one, or a continuous RV uniformly distributed over the interval [0,1], and we can show [63] that $\mathbb{E}\{\Delta_i^{1/b}\} = q^2 + 2q(1-q)b/(b+1)$.
3) *Exponential-interarrivals traffic:* Considering that $L_{\mathrm{p}}\lambda_{\mathrm{p}} \ll 1$, then $p_{\mathrm{T}} \approx L_{\mathrm{p}}\lambda_{\mathrm{p}}$ and $p_{\mathrm{S}} = e^{-2L_{\mathrm{p}}\lambda_{\mathrm{p}}}$. The duty-cycle factor Δ_i is either zero or a uniform RV in the interval [0,1], and we can show [63] that $\mathbb{E}\{\Delta_i^{1/b}\} = (1 - e^{-2L_{\mathrm{p}}\lambda_{\mathrm{p}}})b/(b+1)$.

E. Discussion

Using the results derived in this section, we can obtain insights into the behavior of the throughput as a function of important network parameters, such as the type of propagation characteristics and traffic pattern. In particular, the throughput in the slotted-synchronous and slotted-asynchronous cases can be related as follows. Considering that $b > 1$, we can easily show that $q \leq q^2 + 2q(1-q)b/(b+1)$, with equality iff $q = 0$ or $q = 1$. Therefore, $\mathbb{E}\{\Delta_i^{1/b}\}$ is smaller (or, equivalently, $\mathbb{P}\{\mathsf{SINR} \geq \theta^*\}$ is larger) for the slotted-synchronous case than for the slotted-asynchronous case, regardless of the specific propagation conditions. Furthermore, since $q(1-q) \geq q(1-q)^2$,

we conclude that the throughput $\mathcal{T}$ given in (30) is higher for slotted-synchronous traffic than for slotted-asynchronous traffic. The reason for the higher throughput performance in the synchronous case is that a packet can potentially overlap with only *one packet* transmitted by another node, while in the asynchronous case, it can collide with any of the *two packets* in adjacent time slots.

We can also analyze how the throughput of the probe link depends on the interfering nodes, which are characterized by their spatial density λ and the transmitted power P_{I}. In all the expressions for $\mathbb{P}\{\mathsf{SINR} \geq \theta^*\}$, we can make the parameters λ and P_{I} appear explicitly by noting that if $I \sim \mathcal{S}(\alpha, \beta, \gamma)$, then $\widetilde{I} = \gamma^{-1/\alpha} I \sim \mathcal{S}(\alpha, \beta, 1)$ is a normalized version of I with unit dispersion. Thus, we can for example rewrite (32) as

$$\mathbb{P}\{\mathsf{SINR} \geq \theta^*\} = \mathbb{E}_{\{Z_{0,k}\}}\left\{ F_{\widetilde{I}}\left(\frac{\frac{P_0 \prod_k Z_{0,k}}{r_0^{2b}\theta^*} - N}{P_{\mathrm{I}}\left[\pi\lambda C_{1/b}^{-1}\mathbb{E}\left\{\Delta_i^{1/b}\right\}\prod_k \mathbb{E}\left\{Z_{i,k}^{1/b}\right\}\right]^b} \right) \right\} \tag{40}$$

where $\widetilde{I} \sim \mathcal{S}(\alpha = 1/b, \beta = 1, \gamma = 1)$ only depends on the amplitude loss exponent b. Furthermore, since $F_{\widetilde{I}}(\cdot)$ is monotonically increasing with respect to its argument, we conclude that $\mathbb{P}\{\mathsf{SINR} \geq \theta^*\}$ and therefore the throughput $\mathcal{T}$ is monotonically decreasing with λ and P_{I}. In particular, since $b > 1$, the throughput is more sensitive to an increase in the *spatial density* of the interferers than to an increase in their *transmitter power*. This analysis is valid for any wireless propagation characteristics and traffic pattern.

F. Numerical Results

Fig. 4 shows the dependence of the packet throughput on the transmission probability for various types of packet traffic. We observe that the throughput is higher for slotted-synchronous traffic than for slotted-asynchronous traffic, as demonstrated in Section V-E. Fig. 5 plots the throughput versus the spatial density of interferers for various wireless propagation effects. We observe that the throughput decreases monotonically with the spatial density of the interferers, as also shown in Section V-E.

VI. SPECTRUM OF THE AGGREGATE NETWORK EMISSION

The spectral occupancy and composition of the aggregate RF emission generated by a network is an important consideration in the design of wireless systems. In particular, it is often beneficial to know the spectral properties of the aggregate RF emission generated by all the spatially scattered nodes in the network. This is useful in commercial applications, for example, where communication designers must ensure that the RF emission of the network does not cause interference to other systems operating in overlapping frequency bands. To prevent interference, many commercial networks operate under restrictions which often take the form of spectral masks, imposed by a regulatory agency such as the Federal Communications Commission (FCC). In military applications, on the other hand, the goal is ensure that the presence of the deployed network is not detected by the enemy. If, for example, a sensor network is to be deployed in enemy territory, then the characterization of the aggregate network emission is essential for the design of a covert system.

In this section, we introduce a framework for spectral characterization of the aggregate RF emission of a wireless network [67], [68]. We first characterize the PSD of the

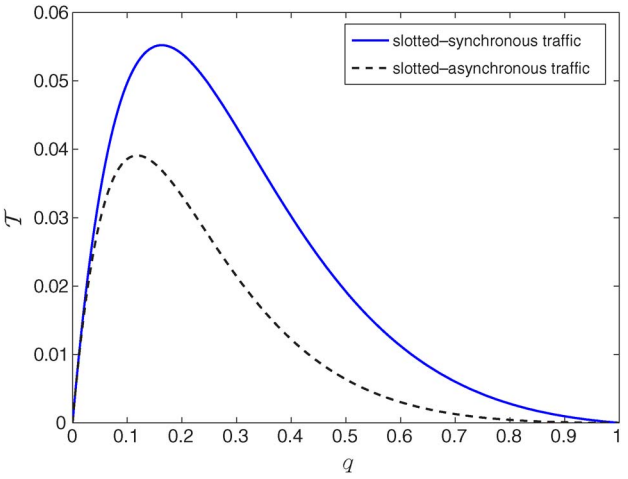

Fig. 4. *Throughput $\mathcal{T}$ versus the transmission probability q, for various types of packet traffic (path loss and Rayleigh fading, $P_0/N = P_{\mathrm{I}}/N = 10$, $\theta^* = 1$, $\lambda = 1\ \mathrm{m}^{-2}$, $b = 2$, $r_0 = 1$ m).*

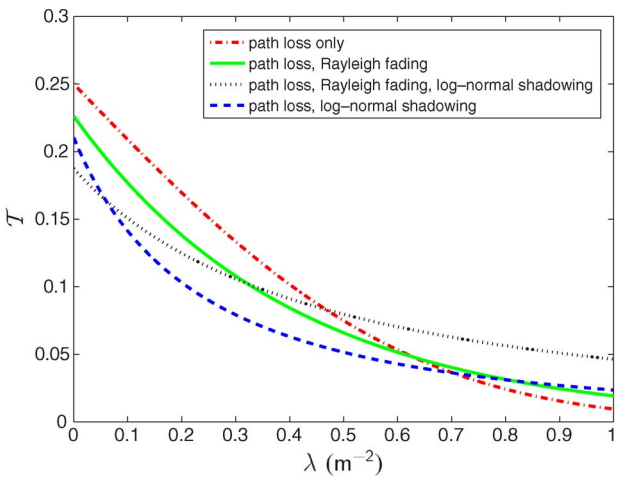

Fig. 5. *Throughput $\mathcal{T}$ versus the interferer spatial density λ, for various wireless propagation characteristics (slotted-synchronous traffic, $P_0/N = P_{\mathrm{I}}/N = 10$, $\theta^* = 1$, $q = 0.5$, $b = 2$, $r_0 = 1$ m, $\sigma_{\mathrm{dB}} = 10$).*

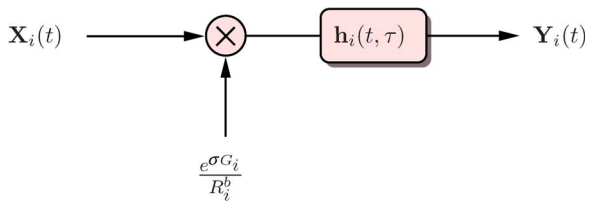

Fig. 6. *Channel model for spectral analysis.*

aggregate emission process $\mathbf{Y}(t)$, measured by the probe receiver in Fig. 1. The spectral characteristics of $\mathbf{Y}(t)$ can be inferred from the knowledge of its PSD. Then, we put forth the concept of spectral outage probability and present some of its applications, including the establishment of spectral regulations and the design of covert military networks. As described in Section II-C, we consider the scenario of slow-varying $\mathcal{P}$, where the analysis is first conditioned on $\mathcal{P}$ to derive a *spectral outage probability*. Other fast-varying propagation effects, such as multipath fading due to local scattering, are averaged out in the analysis.

A. Power Spectral Density of the Aggregate Network Emission

The aggregate network emission at the probe receiver can be characterized by the ELP random process $\mathbf{Y}(t)$, defined as

$$\mathbf{Y}(t) = \sum_{i=1}^{\infty} \mathbf{Y}_i(t) \tag{41}$$

where $\mathbf{Y}_i(t)$ is the received process originated from node i. In the typical case of path loss, log-normal shadowing, and multipath fading, the signal $\mathbf{Y}_i(t)$ in (2) reduces to

$$\mathbf{Y}_i(t) = \frac{e^{\sigma G_i}}{R_i^b} \int \mathbf{h}_i(t,\tau)\mathbf{X}_i(t-\tau)d\tau \tag{42}$$

where $\mathbf{X}_i(t)$ is the ELP transmitted signal and $\mathbf{h}_i(t,\tau)$ is time-varying ELP impulse response of the multipath channel associated with node i. The system model described by (42) is depicted in Fig. 6. Since in this section we are only interested in the aggregate emission of the network, we can ignore the existence of the probe link depicted in Fig. 1. In what follows, we carry out the analysis in ELP, although it can be trivially translated to passband frequencies.

In the remainder of this section, we consider that the transmitted signal $\mathbf{X}_i(t)$ is a wide-sense stationary (WSS) process, such that its autocorrelation function has the form $R_{\mathbf{X}_i}(t_1,t_2) \triangleq \mathbb{E}\{\mathbf{X}_i^*(t_1)\mathbf{X}_i(t_2)\} = R_{\mathbf{X}}(\Delta t)$, where $\mathcal{S}_{\mathbf{X}}(f) \triangleq \mathcal{F}_{\Delta t\to f}\{R_{\mathbf{X}}(\Delta t)\}$.[16] We define the PSD of the process $\mathbf{X}_i(t)$ as $\mathcal{S}_{\mathbf{X}}(f) \triangleq \mathcal{F}_{\Delta t\to f}\{R_{\mathbf{X}}(\Delta t)\}$.[17] Since different nodes operate independently, the processes $\mathbf{X}_i(t)$ are also independent for different i, but the underlying second-order statistics are the same (i.e., the autocorrelation function and the PSD of $\mathbf{X}_i(t)$ do not depend on i).

In terms of the multipath channel, we consider a wide-sense stationary uncorrelated scattering (WSSUS) channel [69]–[73], so that the autocorrelation function of $\mathbf{h}_i(t,\tau)$ can be expressed as

$$\begin{aligned} R_{\mathbf{h}_i}(t_1,t_2,\tau_1,\tau_2) &\triangleq \mathbb{E}\{\mathbf{h}_i^*(t_1,\tau_1)\mathbf{h}_i(t_2,\tau_2)\} \\ &= P_{\mathbf{h}}(\Delta t,\tau_2)\delta(\tau_2-\tau_1) \end{aligned}$$

for some function $P_{\mathbf{h}}(\Delta t,\tau)$. Such channel can be represented in the form of a dense tapped delay line, as a continuum of uncorrelated, randomly scintillating scatterers having WSS statistics. The functions $\mathbf{h}_i(t,\tau)$ are considered to be independent for different nodes i, but the underlying second-order statistics are the same (i.e., the autocorrelation function of $\mathbf{h}_i(t,\tau)$ does not depend on i). WSSUS channels are an important class of practical channels, which simultaneously exhibit wide-sense stationarity in the time variable t and uncorrelated scattering in the delay variable τ.

We now wish to derive the PSD of the aggregate RF emission $\mathbf{Y}(t)$ of the network, and with that purpose we introduce the following theorem.

Theorem 6.1 (WSS and WSSUS Channels): Let $\mathbf{h}(t,\tau)$ denote the time-varying ELP impulse response of a multipath channel, whose autocorrelation function is given by $R_{\mathbf{h}}(t_1,t_2,\tau_1,\tau_2)$. Let $\mathbf{u}(t)$ denote the ELP WSS process that is applied as input to the channel and $\mathbf{z}(t)$ denote the corresponding output process of the channel.

1) If the channel $\mathbf{h}(t,\tau)$ is WSS, i.e., $R_{\mathbf{h}}(t_1,t_2,\tau_1,\tau_2) = R_{\mathbf{h}}(\Delta t,\tau_1,\tau_2)$, then the output $\mathbf{z}(t)$ is WSS and its PSD is given by[18]

$$\mathcal{S}_{\mathbf{z}}(f) = \iint P_{\mathrm{s}}(\nu,\tau_1,\tau_2)\big|_{\nu=f} \overset{f}{*} \left[\mathcal{S}_{\mathbf{u}}(f)e^{j2\pi f(\tau_1-\tau_2)}\right] d\tau_1 d\tau_2 \tag{43}$$

where $P_{\mathrm{s}}(\nu,\tau_1,\tau_2) \triangleq \mathcal{F}_{\Delta t\to\nu}\{R_{\mathbf{h}}(\Delta t,\tau_1,\tau_2)\}$ and $\mathcal{S}_{\mathbf{u}}(f)$ is the PSD of $\mathbf{u}(t)$.

[16] As we will show in the case study of Section VI-C, if $\mathbf{X}_i(t)$ is a train of pulses with a uniformly distributed random delay (which models the asynchronism between emitting nodes), then it is a WSS process.

[17] We use $\mathcal{F}_{x\to y}\{\cdot\}$ to denote the Fourier transform operator, where x and y represent the independent variables in the original and transformed domains, respectively.

[18] We use $\overset{x}{*}$ to denote the convolution operation with respect to variable x.

2) If the channel $\mathbf{h}(t,\tau)$ is WSSUS, i.e., $R_{\mathbf{h}}(t_1,t_2,\tau_1,\tau_2) = P_{\mathbf{h}}(\Delta t,\tau_2)\delta(\tau_2-\tau_1)$ for some function $P_{\mathbf{h}}(\Delta t,\tau)$, then the output $\mathbf{z}(t)$ is WSS and its PSD is given by

$$\mathcal{S}_{\mathbf{z}}(f) = \mathcal{D}_{\mathbf{h}}(\nu)|_{\nu=f} \overset{f}{*} \mathcal{S}_{\mathbf{u}}(f) \tag{44}$$

where $\mathcal{D}_{\mathbf{h}}(\nu) \triangleq \int P_{\mathrm{s}}(\nu,\tau)d\tau$ is the *Doppler power spectrum* of the channel $\mathbf{h}(t,\tau)$, and $P_{\mathrm{s}}(\nu,\tau) \triangleq \mathcal{F}_{\Delta t\to\nu}\{P_{\mathbf{h}}(\Delta t,\tau)\}$ is the *scattering function* of the channel $\mathbf{h}(t,\tau)$.

Proof: See [55]. □

In the specific context of (42), the theorem implies that $\mathbf{Y}_i(t)$ is WSS and thus the aggregate network emission $\mathbf{Y}(t)$ is also WSS. Furthermore, the PSD of $\mathbf{Y}_i(t)$ is given by

$$\mathcal{S}_{\mathbf{Y}_i}(f) = \frac{e^{2\sigma G_i}}{R_i^{2b}}\left[\mathcal{D}_{\mathbf{h}}(f) * \mathcal{S}_{\mathbf{X}}(f)\right] \tag{45}$$

where $\mathcal{D}_{\mathbf{h}}(f)$ is the Doppler power spectrum of the time-varying multipath channel $\mathbf{h}_i(t,\tau)$, and $\mathcal{S}_{\mathbf{X}}(f)$ is the PSD of the transmitted signal $\mathbf{X}_i(t)$. Because the processes $\mathbf{Y}_i(t)$ associated with different emitting nodes i are statistically independent when conditioned on $\mathcal{P}$, we can write

$$\mathcal{S}_{\mathbf{Y}}(f) = \sum_{i=1}^{\infty} \mathcal{S}_{\mathbf{Y}_i}(f). \tag{46}$$

Combining (45) and (46), we obtain the desired conditional PSD of the aggregate network emission $\mathbf{Y}(t)$ as

$$\mathcal{S}_{\mathbf{Y}}(f,\mathcal{P}) = A\left[\mathcal{D}_{\mathbf{h}}(f) * \mathcal{S}_{\mathbf{X}}(f)\right] \tag{47}$$

where A is defined as

$$A \triangleq \sum_{i=1}^{\infty} \frac{e^{2\sigma G_i}}{R_i^{2b}}. \tag{48}$$

Note that in (47), we explicitly indicated the conditioning of $\mathcal{S}_{\mathbf{Y}}$ on $\mathcal{P}$. Since $\mathcal{S}_{\mathbf{Y}}(f,\mathcal{P})$ depends on $\mathcal{P}$, it can be viewed, for a fixed f, as an RV whose value is different for each realization of $\mathcal{P}$.[19] Lastly, note that since A in (48) depends on $\mathcal{P}$ (i.e., $\{R_i\}_{i=1}^{\infty}$ and $\{G_i\}_{i=1}^{\infty}$), it can be seen as an RV whose value is different for each realization of $\mathcal{P}$. The distribution of the A can be determined from Corollary 3.2, setting $P_i = e^{2\sigma G_i}$. Then, it follows that A has a skewed stable distribution given by

$$A \sim \mathcal{S}\left(\alpha_A = \frac{1}{b}, \beta_A = 1, \gamma_A = \pi\lambda C_{1/b}^{-1} e^{2\sigma^2/b^2}\right) \tag{49}$$

where $b > 1$ and C_x is defined in (12). This distribution is plotted in Fig. 7 for different values of b and λ.

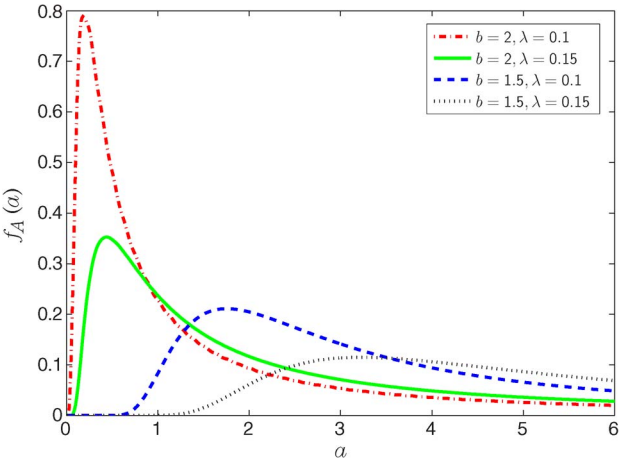

Fig. 7. ***PDF of A for different amplitude loss exponents b and interferer densities λ ($\sigma_{\mathrm{dB}} = 10$). Stable laws are a direct generalization of Gaussian distributions and include other densities with heavier (algebraic) tails.***

B. Spectral Outage Probability

In the proposed quasi-static scenario, the PSD of the aggregate network emission $\mathcal{S}_{\mathbf{Y}}(f,\mathcal{P})$ is a function of the random node positions and shadowing $\mathcal{P}$. Then, with some probability, $\mathcal{P}$ is such that the spectrum of the aggregate emission is too high in some frequency band of interest, thus causing an outage in that frequency band. This leads to the concept of *spectral outage probability*, which we denote by $P_{\mathrm{out}}^{\mathrm{s}}(f)$ and generally define as [67], [68]

$$P_{\mathrm{out}}^{\mathrm{s}}(f) \triangleq \mathbb{P}_{\mathcal{P}}\{\mathcal{S}_{\mathbf{Y}}(f,\mathcal{P}) > m(f)\} \tag{50}$$

where $\mathcal{S}_{\mathbf{Y}}(f,\mathcal{P})$ is the random PSD of the aggregate network emission $\mathbf{Y}(t)$ and $m(f)$ is some spectral mask determining the outage (or detection) threshold at the receiver. The SOP is a frequency-dependent quantity and, in the case of slow-varying $\mathcal{P}$, is a more insightful metric than the PSD averaged over $\mathcal{P}$. Note that this definition is applicable in general to any emission model: the spectral

[19] $\mathcal{S}_{\mathbf{Y}}(f,\mathcal{P})$ is in fact a random process whose sample paths evolve in *frequency* instead of *time*. For each realization $\mathcal{P} = \mathcal{P}_0$, we obtain a sample path $\mathcal{S}_{\mathbf{Y}}(f,\mathcal{P}_0)$ that is a function of f; for a fixed frequency $f = f_0$, $\mathcal{S}_{\mathbf{Y}}(f_0,\mathcal{P})$ is a RV.

outage probability $P_{\text{out}}^{\text{s}}(f)$ represents the probability that the PSD of the aggregate network emission, measured at an arbitrary location in the plane and at a particular frequency f, exceeds some predetermined mask.

For the signal model considered in this section, $P_{\text{out}}^{\text{s}}(f)$ can be derived by substituting (47) into the general definition of SOP in (50), leading to

$$P_{\text{out}}^{\text{s}}(f) = \mathbb{P}\left\{A > \frac{m(f)}{\mathcal{D}_{\mathbf{h}}(f) * \mathcal{S}_{\mathbf{X}}(f)}\right\} = 1 - F_A\left(\frac{m(f)}{\mathcal{D}_{\mathbf{h}}(f) * \mathcal{S}_{\mathbf{X}}(f)}\right) \tag{51}$$

where $F_A(\cdot)$ is the cdf of the stable RV A, whose distribution is given in (49).

In what follows, we present two possible applications of the SOP.

1) Application to Spectral Regulations: The concept of SOP can provide a radically different way to establish spectral regulations. Current regulations and standards (e.g., FCC Part 15 or IEEE 802.11) impose a spectral mask on the PSD *at the transmitter*, and the type of mask often depends on the environment in which the devices are operated (e.g., indoor or outdoor). The purpose of this mask is to limit RF emissions generated by a terminal and to protect other services that operate in dedicated bands (e.g., GPS, public safety, and cellular systems). However, the *transmitted* PSD is usually not representative of the aggregate PSD *at the victim receiver* due to the random propagation effects (multipath fading and shadowing) and the random position of the emitting nodes. Thus, spectral regulations that are based only on the transmitted PSD do not necessarily protect a victim receiver against interference.

The approach proposed here is radically different, in the sense that the spectral mask is defined at the victim receiver, not at the transmitter [74]. In effect, the mask $m(f)$ introduced in (50) represents the outage threshold with respect to the *accumulated PSD at the receiver*, not the individual PSD at the transmitter (this follows from the fact that $\mathcal{S}_{\mathbf{Y}}(f, \mathcal{P})$ is measured at an arbitrary location in the plane, where a probe receiver could be located). Therefore, the received aggregate spectrum $\mathcal{S}_{\mathbf{Y}}(f, \mathcal{P})$ and the corresponding $P_{\text{out}}^{\text{s}}(f)$ can be used to characterize and control the network's RF emissions more effectively, since they not only consider the aggregate effect of all emitting nodes at an arbitrary receiver location but also incorporate the random propagation effects and random node positions. Furthermore, the use of different masks for indoor or outdoor environments is no longer necessary, since the environment is already accounted for in our model by parameters such as the amplitude loss exponent b, the spatial density λ of the emitting nodes, and the shadowing coefficient σ.

2) Application to Covert Military Networks: In military applications, the goal is to ensure that the presence of the deployed network is not detected by the enemy. If, for example, a surveillance network is to be deployed in enemy territory, then the characterization of its aggregate emission is essential for the design of a covert network with low probability of detection. In such application, the function $m(f)$ in (50) can be interpreted as the frequency-dependent mask, which determines the *detection threshold* (not the outage threshold as before) [75]. In other words, if the aggregate spectral density $\mathcal{S}_{\mathbf{Y}}(f, \mathcal{P})$ measured at a given location exceeds the mask $m(f)$, then the presence of the deployed network may be detected by the enemy.

C. Numerical Results

We now present a case study to quantify the spectral densities and outage probabilities derived in the previous section. We also illustrate their dependence on the various parameters involved, such as the transmitted pulse shape, spectral mask, transmitted power, and spatial density of the emitting nodes. For all numerical examples, we consider that the emitting nodes employ a two-dimensional modulation (e.g., M-PSK or M-QAM), such that transmitted signal $\mathbf{X}_i(t)$ can be written for all t as

$$\mathbf{X}_i(t) = \sum_{n=-\infty}^{+\infty} \mathbf{a}_{i,n} g(t - nT - D_i) \tag{52}$$

where the sequence $\{\mathbf{a}_{i,n}\}_{n=-\infty}^{+\infty}$ represents the stream of complex symbols transmitted by node i, assumed to be i.i.d. in n and zero mean, for simplicity; $g(t)$ is a real, baseband, unit-energy shaping pulse, defined for all values of t; T is the symbol period; and $D_i \sim \mathcal{U}(0, T)$ is a random delay representing the asynchronism between different emitting nodes. The type of constellation employed by the emitting nodes is captured by the statistics of the symbols $\{\mathbf{a}_{i,n}\}$.[20] Note that the process $\mathbf{X}_i(t)$ in (52) is WSS, as required by Theorem 6.1.[21] The PSD of $\mathbf{X}_i(t)$ is then given by [78]–[80]

$$\mathcal{S}_{\mathbf{X}}(f) = P_{\text{tx}} |G(f)|^2 \tag{53}$$

where $P_{\text{tx}} = \mathbb{E}\{|\mathbf{a}_{i,n}|^2\}/T$ is the power transmitted by each emitting node and $G(f) = \mathcal{F}\{g(t)\}$.

In terms of the multipath channel, we consider for simplicity that $\mathbf{h}(t, \tau)$ is time-invariant such that it does

[20]Note that each complex symbol $\mathbf{a}_{i,n} = a_{i,n} e^{j\theta_{i,n}}$ can be represented in the in-phase/quadrature (IQ) plane by a constellation point with amplitude $a_{i,n}$ and phase $\theta_{i,n}$.

[21]This can be shown in the following way: first, if we deterministically set D_i to zero in (52), the resulting process $\widetilde{\mathbf{X}}_i(t)$ is wide-sense cyclostationary (WSCS) with period T [76], [77]; then, since $\mathbf{X}_i(t) = \widetilde{\mathbf{X}}_i(t - D_i)$, where $D_i \sim \mathcal{U}(0, T)$ and is independent of everything else, it follows that $\mathbf{X}_i(t)$ is WSS.

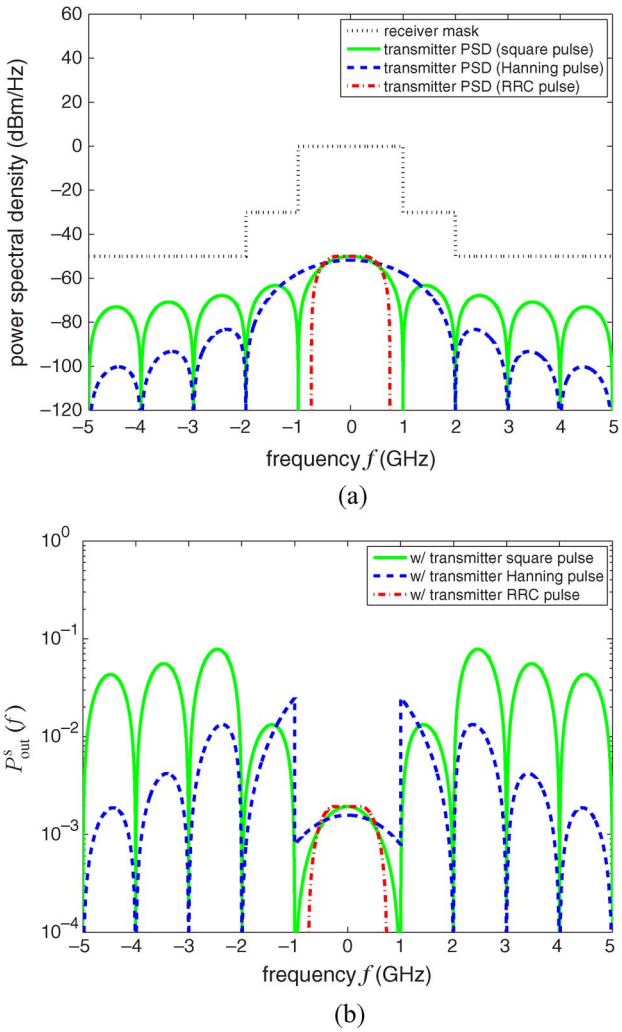

Fig. 8. *Effect of the transmitted baseband pulse shape $g(t)$ on the PSD and the outage probability $P^s_{out}(f)$ ($P_{tx} = 10$ dBm, $T = 10^{-9}$ s, $\lambda = 0.1$ m^{-2}, $b = 2$, $\sigma_{dB} = 10$, RRC pulse with rolloff factor 0.5). (a) PSD of the individual transmitted signal versus frequency (bottom curves) for various pulse shapes $g(t)$. The pulses are normalized so that the transmitted signals have the same power P_{tx}. The piecewise-constant spectral mask $m(f)$ (top curve) determines the outage threshold at the receiver. (b) Spectral outage probability $P^s_{out}(f)$ versus frequency for the piecewise-constant mask $m(f)$ shown in (a).*

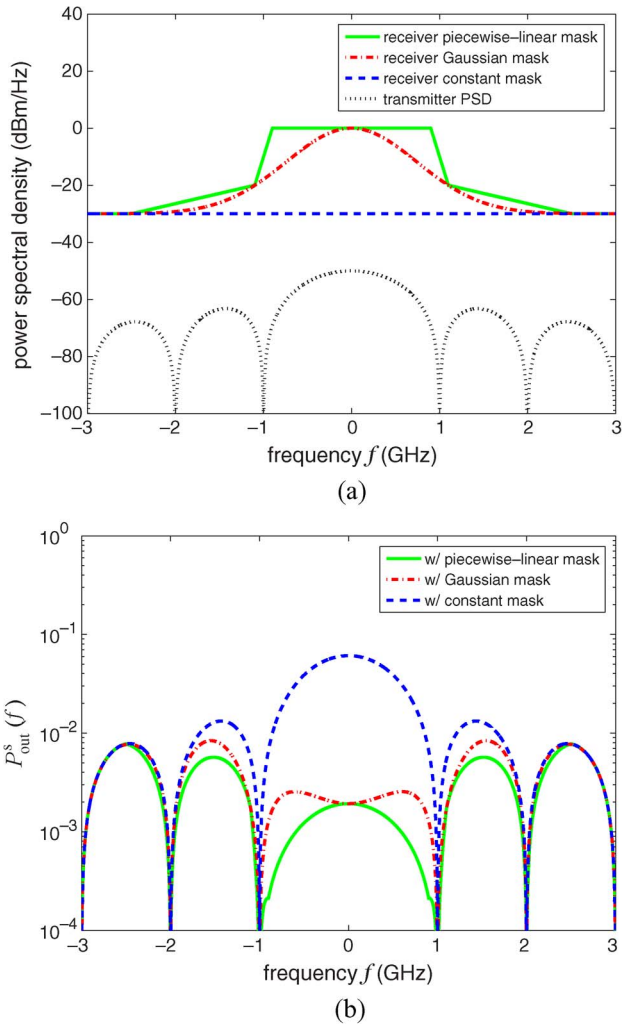

Fig. 9. *Effect of the spectral mask shape $m(f)$ on the outage probability $P^s_{out}(f)$ (square $g(t)$, $P_{tx} = 10$ dBm, $T = 10^{-9}$ s, $\lambda = 0.1$ m^{-2}, $b = 2$, $\sigma_{dB} = 10$). (a) Plot of various spectral masks $m(f)$, which define the outage threshold at the receiver (top curves). Also shown is the PSD of the individual transmitted signal versus frequency (bottom curve). (b) Spectral outage probability $P^s_{out}(f)$ versus frequency for the various masks $m(f)$ shown in (a).*

not introduce any Doppler shifts, i.e., $\mathcal{D}_{\mathbf{h}}(\nu) = \delta(\nu)$.[22] Substituting the expressions for $\mathcal{S}_{\mathbf{X}}(f)$ and $\mathcal{D}_{\mathbf{h}}(\nu)$ in (51), we obtain the SOP as

$$P^s_{out}(f) = 1 - F_A\left(\frac{m(f)}{P_{tx}|G(f)|^2}\right). \tag{54}$$

[22]For typical node speeds or channel fluctuations, the frequencies of the Doppler shifts are on the order of few kilohertz [73]. As a consequence, when the considered $\mathbf{X}_i(t)$ is UWB, $\mathcal{D}_{\mathbf{h}}(\nu)$ can be well approximated by a Dirac-delta function.

Fig. 8 shows that for a fixed spectral mask $m(f)$, the SOP can be highly dependent on the pulse shape $g(t)$, such as square, Hanning, or root raised-cosine (RRC) pulse. In fact, $P^s_{out}(f)$ is a nonlinear function of $|G(f)|$, where the nonlinearity is determined in part by the cdf $F_A(\cdot)$ of the stable RV A, as shown in (54). Thus, the SOP can be used as a criterion for designing the pulse shape: for example, we may wish to determine the baseband pulse $g(t)$ and transmitted power P_{tx} such that $\max_f P^s_{out}(f) \le p^*$, where p^* is some target outage probability which must be satisfied at all frequencies.

Fig. 9 shows that for a fixed pulse shape $g(t)$, $P^s_{out}(f)$ can significantly depend on the spectral mask $m(f)$ (e.g., piecewise-linear, Gaussian, or constant mask). Since

$P^{s}_{\text{out}}(f)$ accounts for both $G(f)$ and $m(f)$, it quantifies the compatibility of the transmitted pulse shape with the spectral restrictions imposed through $m(f)$.

VII. COEXISTENCE BETWEEN UWB AND NB SYSTEMS

The increasing proliferation of heterogeneous communication devices sharing the same frequency bands makes mutual interference a key issue, in order to ascertain whether their coexistence is possible. For example, UWB signals, which occupy extremely large bandwidths, usually operate as an underlay system with other existing, licensed and unlicensed, NB radio systems [81]–[85]. Because of their characteristics, UWB systems are considered among key technologies in the context of cognitive radio [86]–[88]. As a result, the deployment of UWB systems requires that they coexist and contend with a variety of interfering signals. Thus, they must be designed to account for two fundamental aspects: 1) UWB devices must not cause harmful interference to licensed wireless services and existing NB systems (e.g., GPS, GSM, UMTS, 3G, Bluetooth, and WLAN), and 2) UWB devices must be robust and able to operate in the presence of interference caused by both NB systems and other UWB-based nodes.

The framework proposed in this paper enables the characterization of coexistence in heterogeneous wireless networks, and captures all the essential physical parameters that impact UWB and NB network interference. In this section, we consider an application of the framework to the scenario of NB communication in the presence of UWB interferers [56], [89]. We first determine the statistical distribution of the aggregate UWB interference, which naturally leads to the characterization of the corresponding error probability. The application of the proposed framework to the case of UWB communication in the presence of NB interferers is considered in [56], [90].

The proposed spatial model is depicted in Fig. 1, where the interferers are UWB transmitters scattered in the two-dimensional plane, according to a spatial Poisson process with density λ_{U}. In terms of transmission characteristics of nodes, we consider the case where the UWB interferers operate asynchronously and independently, using the same power P_{U}. The signal $s_i^{\text{U}}(t)$ transmitted by the ith UWB interferer can be described as

$$s_i^{\text{U}}(t) = \sqrt{E_{\text{U}}} \sum_{n=-\infty}^{\infty} a_{i,n}^{\text{U}} w_i(t - nT_{\text{U}} - D_i) \tag{55}$$

where E_{U} is the average transmitted symbol energy; $w_i(t)$ is the unit-energy symbol waveform[23]; $a_{i,n}^{\text{U}} \in \{-1, 1\}$ is the nth transmitted symbol of the ith UWB interferer; T_{U} is the symbol period; and $D_i \sim \mathcal{U}(0, T_{\text{U}})$[24] is a random delay modeling the asynchronism between nodes.

The signal transmitted by the NB probe transmitter can be written as

$$s_{\text{N}}(t) = \sqrt{2E_{\text{N}}} \sum_{n=-\infty}^{\infty} a_n^{\text{N}} g(t - nT_{\text{N}}) \cos\left(2\pi f_{\text{N}} t + \theta_n^{\text{N}}\right) \tag{56}$$

where E_{N} is the average transmitted symbol energy; $g(t)$ is a unit-energy pulse-shaping waveform satisfying the Nyquist criterion; $a_n^{\text{N}} e^{j\theta_n^{\text{N}}}$ is the nth transmitted NB symbol, belonging to a constellation $\mathcal{C}^{\text{N}} = \{\mathbf{s}_1^{\text{N}}, \ldots, \mathbf{s}_M^{\text{N}}\}$, and satisfying $\mathbb{E}\{|a_n^{\text{N}}|^2\} = 1$; and f_{N} is the carrier frequency of the NB signal.

To account for the propagation characteristics, we consider that the signal transmitted by the ith UWB interferer experiences a frequency-selective multipath channel with impulse response

$$\widetilde{h}_i^{\text{U}}(t) = \frac{k_{\text{U}}}{R_i^{b_{\text{U}}}} e^{\sigma_{\text{U}} G_i} h_i(t) \tag{57}$$

where

$$h_i(t) = \sum_{q=1}^{L} h_{i,q} \delta(t - \tau_{i,q}) \tag{58}$$

with $\{h_{i,q}\}_{q=1}^{L}$ and $\{\tau_{i,q}\}_{q=1}^{L}$ representing, respectively, the amplitudes and delays (with arbitrary statistics) of the L paths. In addition, we normalize the PDP of the channel such that $\sum_{q=1}^{L} \mathbb{E}\{h_{i,q}^2\} = 1$.[25] We assume the shadowing and fading to be independent for different interferers i, and approximately constant during at least one symbol interval.

On the other hand, the signal transmitted by the NB node experiences a frequency-flat multipath channel with

[23]Note that $w_i(t)$ itself may be composed of many monocycles, and depending on its choice, can be used to represent both direct-sequence (DS) or time-hopping (TH) spread spectrum signals [84].

[24]We use $\mathcal{U}(a, b)$ to denote a real uniform distribution in the interval $[a, b]$.

[25]For strict consistency with the linear time-varying (LTV) description in (3), the impulse response in (58) would be written as $h_i(t, \tau) = \sum_{q=1}^{L} h_{i,q}(t)\delta(\tau - \tau_{i,q}(t))$. For a slow-varying channel, $\tau_{i,q}(t) \approx \tau_{i,q}$, $\tau_{i,q}(t) \approx \tau_{i,q}$, and $h_i(t, \tau)$ does not depend on t, which corresponds to a linear time-invariant (LTI) system. In such case, we proceed as is usually done in the literature by dropping the variable t and replacing τ with t. Note that such LTI impulse response is applicable to error probability analysis, since the interval of interest for symbol detection is typically much smaller than the coherence time of the channel. On the other hand, an LTI impulse response is generally *not* applicable to the spectral analysis of Section VI, since the interval of interest is much larger than the coherence time of the channel, and therefore an LTV representation is needed.

impulse response

$$\widetilde{h}_{\mathrm{N}}(t) = \frac{k_{\mathrm{N}}}{r_0^{b_{\mathrm{N}}}} \alpha_0 e^{\sigma_{\mathrm{N}} G_0} \delta(t - \tau_0) \tag{59}$$

where α_0 is an amplitude factor with Nakagami-m distribution (normalized so that $\mathbb{E}\{\alpha_0^2\} = 1$), and τ_0 is the time delay introduced by the channel. For generality, (57) and (59) can accommodate different path loss parameters for the UWB signals $(k_{\mathrm{U}}, b_{\mathrm{U}})$ and the NB signal $(k_{\mathrm{N}}, b_{\mathrm{N}})$, as well as different shadowing parameters σ_{N} and σ_{U}.

As described in Section II-C, we consider the scenario of slow-varying $\mathcal{P}$, where the analysis is first conditioned on $\mathcal{P}$ to derive an *error outage probability*. Other fast-varying propagation effects, such as multipath fading due to local scattering, are averaged out in the analysis.

A. Signals and Interference Representation

Under the system model described in Section II, the aggregate signal $z(t)$ at the NB victim receiver can be written as

$$z(t) = d(t) + y(t) + n(t)$$

where $d(t) = [\sqrt{2E_{\mathrm{N}}} a_0^{\mathrm{N}} g(t) \cos(2\pi f_{\mathrm{N}} t + \theta_0^{\mathrm{N}})] * \widetilde{h}_{\mathrm{N}}(t)$ is the desired signal from the NB transmitter corresponding to symbol $n = 0$[26]; $y(t) = \sum_{i=1}^{\infty} s_i^{\mathrm{U}}(t) * \widetilde{h}_i^{\mathrm{U}}(t)$ is the aggregate network interference; and $n(t)$ is the AWGN with two-sided power spectral density $N_0/2$, and independent of $y(t)$. By performing the indicated convolutions, we can further express the desired signal as[27]

$$d(t) = \frac{k_{\mathrm{N}} \alpha_0 e^{\sigma_{\mathrm{N}} G_0}}{r_0^{b_{\mathrm{N}}}} \sqrt{2E_{\mathrm{N}}} a_0^{\mathrm{N}} g(t) \cos\left(2\pi f_{\mathrm{N}} t + \theta_0^{\mathrm{N}}\right)$$

and the aggregate interference as

$$y(t) = \sqrt{E_{\mathrm{U}}} \sum_{i=1}^{\infty} \frac{k_{\mathrm{U}} e^{\sigma_{\mathrm{U}} G_i}}{R_i^{b_{\mathrm{U}}}} \sum_{n=-\infty}^{\infty} a_{i,n}^{\mathrm{U}} v_i(t - \widetilde{D}_{i,n})$$

where $v_i(t) = w_i(t) * h_i(t)$, and $\widetilde{D}_{i,n} \triangleq nT_{\mathrm{U}} + D_i$.

The NB receiver demodulates the aggregate signal $z(t)$ using a conventional in-phase/quadrature (IQ) detector. This can be achieved by projecting $z(t)$ onto the orthonormal set $\{\psi_1(t) = \sqrt{2}g(t)\cos(2\pi f_{\mathrm{N}} t), \psi_2(t) = -\sqrt{2}g(t)\sin(2\pi f_{\mathrm{N}} t)\}$. If we let $\psi(t) = \psi_1(t) + \jmath\psi_2(t) = \sqrt{2}g(t)e^{-\jmath 2\pi f_{\mathrm{N}} t}$, we can write

$$\begin{aligned}\mathbf{Z} &= \int_{-\infty}^{+\infty} z(t)\psi(t)dt \\ &= \frac{k_{\mathrm{N}} \alpha_0 e^{\sigma_{\mathrm{N}} G_0}}{r_0^{b_{\mathrm{N}}}} \sqrt{E_{\mathrm{N}}} a_0^{\mathrm{N}} e^{\jmath\theta_0^{\mathrm{N}}} + \mathbf{Y} + \mathbf{N}\end{aligned} \tag{60}$$

where the distribution of $\mathbf{N}$ is given by[28]

$$\mathbf{N} \sim \mathcal{N}_{\mathrm{c}}(0, N_0). \tag{61}$$

Furthermore, $\mathbf{Y} = \int_{-\infty}^{+\infty} y(t)\psi(t)dt$ can be expressed as

$$\mathbf{Y} = \sum_{i=1}^{\infty} \frac{e^{\sigma_{\mathrm{U}} G_i} \mathbf{X}_i}{R_i^{b_{\mathrm{U}}}} \tag{62}$$

where

$$\begin{aligned}\mathbf{X}_i &= X_{i,1} + \jmath X_{i,2} \\ &= k_{\mathrm{U}} \sqrt{E_{\mathrm{U}}} \sum_{n=-\infty}^{\infty} a_{i,n}^{\mathrm{U}} \int_{-\infty}^{+\infty} v_i(t - \widetilde{D}_{i,n})\psi(t)dt.\end{aligned} \tag{63}$$

Note that both $\mathbf{H}_i(f) \triangleq \mathcal{F}\{h_i(t)\}$ and $\mathbf{W}_i(f) \triangleq \mathcal{F}\{w_i(t)\}$ are Fourier transforms of UWB signals, and therefore are approximately constant over the frequencies of the NB signal. As a result, we can show [89] that (63) reduces to

$$\mathbf{X}_i = k_{\mathrm{U}} \sqrt{2E_{\mathrm{U}}} \mathbf{W}_i(f_{\mathrm{N}}) \mathbf{H}_i(f_{\mathrm{N}}) \sum_{n=-\infty}^{\infty} a_{i,n}^{\mathrm{U}} g(\widetilde{D}_{i,n}) e^{-\jmath 2\pi f_{\mathrm{N}} \widetilde{D}_{i,n}}. \tag{64}$$

Note that effective range of the summation of n in (64) depends on the duration of the shaping pulse $g(t)$ relative to T_{U}. In effect, in the usual case where $g(t)$ decreases to 0 as $t \to \pm\infty$, the r.v.'s $g(\widetilde{D}_{i,n})$ become increasingly small since $\widetilde{D}_{i,n}$ grows as n increases, and so the sum in n can be truncated.

B. Distribution of the Aggregate UWB Interference

The distribution of the aggregate UWB interference $\mathbf{Y}$ plays an important role in the evaluation of the error probability of the victim link. Based on the Kullback-Leibler divergence [56], [91], it can be shown that the $\mathcal{P}$-conditioned distribution of the aggregate interference $\mathbf{Y}$ in (62) can be accurately approximated by a circularly

[26] To derive the error probability of the NB victim link, we only need to analyze a single NB symbol.

[27] In what follows, we assume that the NB receiver can perfectly estimate τ_0, and thus perfectly synchronize with the desired signal. As a result, we can set $\tau_0 = 0$ in the remaining analysis.

[28] We use $\mathcal{N}_{\mathrm{c}}(0, \sigma^2)$ to denote a circularly symmetric (CS) complex Gaussian distribution, where the real and imaginary parts are i.i.d. $\mathcal{N}(0, \sigma^2/2)$.

symmetric (CS) complex Gaussian r.v. with the same variance as (62), i.e.,

$$\mathbf{Y} \overset{|\mathcal{P}}{\sim} \mathcal{N}_c(0, 2AV_X) \tag{65}$$

where A is defined as

$$A \triangleq \sum_{i=1}^{\infty} \frac{e^{2\sigma_U G_i}}{R_i^{2b_U}} \tag{66}$$

and[29]

$$V_X \triangleq \mathbb{V}\{\mathsf{X}_{i,k}\}. \tag{67}$$

Note that since A in (66) depends on $\mathcal{P}$ (i.e., $\{R_i\}_{i=1}^{\infty}$ and $\{G_i\}_{i=1}^{\infty}$), it can be seen as a r.v. whose value is different for each realization of $\mathcal{P}$. The distribution of the A can be determined from Corollary 3.2, setting $P_i = e^{2\sigma_U G_i}$. Then, it follows that A has a skewed stable distribution given by

$$A \sim \mathcal{S}\left(\alpha_A = \frac{1}{b_U}, \quad \beta_A = 1, \quad \gamma_A = \pi\lambda_U C_{1/b_U}^{-1} e^{2\sigma_U^2/b_U^2}\right) \tag{68}$$

where $b_U > 1$, and C_α is defined in (12).

C. Error Probability

In a quasi-static scenario of slow-varying $\mathcal{P}$, it is insightful to analyze the error probability conditioned on $\mathcal{P}$, as well as on the shadowing G_0 of the NB victim link. We denote this conditional symbol error probability by $P_e(G_0, \mathcal{P})$.[30]

To derive the conditional error probability, we employ the results of Section VII-B for the distribution of the aggregate UWB interference $\mathbf{Y}$. Specifically, using (61) and (65), the received signal $\mathbf{Z}$ in (60) can be rewritten as

$$\mathbf{Z} = \frac{k_N \alpha_0 e^{\sigma_N G_0}}{r_0^{b_N}} \sqrt{E_N} a_0^N e^{\jmath\theta_0^N} + \widetilde{\mathbf{N}} \tag{69}$$

where

$$\widetilde{\mathbf{N}} = \mathbf{Y} + \mathbf{N} \overset{|\mathcal{P}}{\sim} \mathcal{N}_c(0, 2AV_X + N_0) \tag{70}$$

and A was defined in (66). Our framework has thus reduced the analysis of NB communication in the presence of UWB network interference to a Gaussian problem, where the combined noise $\widetilde{\mathbf{N}}$ is Gaussian when conditioned on the location of the UWB interferers.

The corresponding error probability $P_e(G_0, \mathcal{P})$ can be found by taking the well-known error probability expressions for coherent detection of two-dimensional modulations in the presence of AWGN and fast fading [92]–[96], but using $2AV_X + N_0$ instead of N_0 for the total noise variance. Note that this substitution is valid for any two-dimensional modulation, allowing the traditional results to be extended to include the effect of UWB network interference. For the case where the NB transmitter employs an arbitrary signal constellation in the IQ-plane and the fading has a Nakagami-m distribution, the conditional symbol error probability $P_e(G_0, \mathcal{P})$ is given by

$$P_e(G_0, \mathcal{P}) = \sum_{k=1}^{M} p_k \sum_{l \in \mathcal{B}_k} \frac{1}{2\pi} \times \int_0^{\phi_{k,l}} \left(1 + \frac{w_{k,l}}{4m \sin^2(\theta + \psi_{k,l})} \eta_A\right)^{-m} d\theta \tag{71}$$

where

$$\eta_A = \frac{k_N^2 e^{2\sigma_N G_0} E_N}{r_0^{2b_N}(2AV_X + N_0)} \tag{72}$$

is the received SINR averaged over the fast fading; M is the NB constellation size; $\{p_k\}_{k=1}^{M}$ are the NB symbol probabilities; $\mathcal{B}_k$, $\phi_{k,l}$, $w_{k,l}$, and $\psi_{k,l}$ are the parameters that describe the geometry of the NB constellation (see Fig. 10); A is defined in (66) and distributed according to (68); and V_X is defined in (67). The result in (71) can be easily generalized to the scenario where the victim link employs diversity techniques, using the methods described in [94]–[98].

When the NB transmitter employs M-PSK and M-QAM modulations with equiprobable symbols, (71) is equivalent to[31]

$$P_e^{\mathrm{MPSK}}(G_0, \mathcal{P}) = \mathcal{I}_A\left(\frac{M1}{M}\pi, \sin^2\left(\frac{\pi}{M}\right)\right) \tag{73}$$

and

$$P_e^{\mathrm{MQAM}}(G_0, \mathcal{P}) = 4\left(1 - \frac{1}{\sqrt{M}}\right) \cdot \mathcal{I}_A\left(\frac{\pi}{2}, \frac{3}{2(M-1)}\right) - 4\left(1 - \frac{1}{\sqrt{M}}\right)^2 \cdot \mathcal{I}_A\left(\frac{\pi}{4}, \frac{3}{2(M-1)}\right) \tag{74}$$

[29] We use $\mathbb{V}\{\cdot\}$ to denote the variance operator.

[30] The notation $P_e(X, Y)$ is used as a shorthand for $\mathbb{P}\{\text{error}|X, Y\}$.

[31] In this paper, we implicitly assume that M-QAM employs a square signal constellation with $M = 2^n$ points (n even).

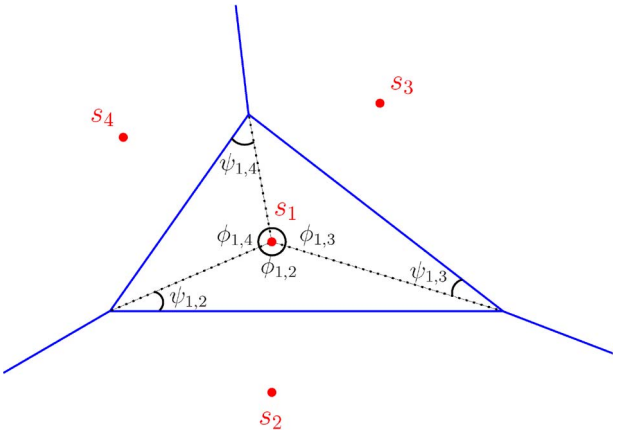

Fig. 10. *Typical decision region associated with symbol s_1. In general, for a constellation $\mathcal{C} = \{s_1, \ldots, s_M\}$ with signal points $s_k = |s_k|e^{j\xi_k}$ and with $\zeta_k \triangleq |s_k|^2/\mathbb{E}\{|s_k|^2\}$, $k = 1 \ldots M$, four parameters are required to compute the error probability: $\phi_{k,l}$ and $\psi_{k,l}$ are the angles that describe the decision region corresponding to s_k (as depicted); $\mathcal{B}_k$ is the set consisting of the indexes for the signal points that share a decision boundary with s_k (in the example, $\mathcal{B}_1 = \{2, 3, 4\}$); and $w_{k,l} \triangleq \zeta_k + \zeta_l - 2\sqrt{\zeta_k \zeta_l}\cos(\xi_k - \xi_l)$.*

where the integral $\mathcal{I}_A(x, g)$ is given by

$$\mathcal{I}_A(x, g) = \frac{1}{\pi}\int_0^x \left(1 + \frac{g}{m\sin^2\theta}\eta_A\right)^{-m} d\theta. \qquad (75)$$

In the general expression given in (71) and (72), the network interference is accounted for by the term $2AV_X$, where A depends on the spatial distribution of the UWB interferers and propagation characteristics of the medium, while V_X depends on the transmission characteristics of the UWB interferers. Since $2AV_X$ simply adds to N_0, we conclude that the effect of the interference on the conditional error probability is simply an increase in the noise level, a fact which is intuitively satisfying. Furthermore, note that the modulation of the UWB interfering nodes only affects the term V_X, while the modulation of the NB link affects the *type* of error probability expression, leading to forms such as (73) or (74).

In our quasi-static model, the conditional error probability $P_e(G_0, \mathcal{P})$ is seen to be a function of the slow-varying interferer positions and shadowing (i.e., G_0 and $\mathcal{P}$). Since these quantities are random, $P_e(G_0, \mathcal{P})$ is itself a r.v. Then, with some probability, G_0 and $\mathcal{P}$ are such that the conditional error probability of the victim link is above some target p^*. The system is said to be *in outage*, and the error outage probability is

$$P_{\text{out}}^{\text{e}} = \mathbb{P}_{G_0,\mathcal{P}}(P_e(G_0, \mathcal{P}) > p^*) \qquad (76)$$

In the case of slow-varying interferer positions, the error outage probability is a more meaningful metric than the error probability averaged over $\mathcal{P}$, as discussed in Section II-C.

D. Numerical Results

We now particularize the general analysis developed in the previous sections, using a simple case study of a BPSK NB victim link subject to the DS-BPAM UWB interferers. In this scenario, the signal $s_i(t)$ transmitted by the ith interferer in (55) becomes

$$s_i^{\text{U}}(t) = \sqrt{E_{\text{U}}}\sum_n a_{i,n}^{\text{U}} w_i(t - nN_sT_f - D_i)$$

where the unit-energy waveform $w_i(t)$ for each bit is given by

$$w_i(t) = \sum_{k=0}^{N_s-1} c_{i,k}p(t - kT_f).$$

In these equations, N_s is the number of monocycles required to transmit a single information bit $a_{i,n}^{\text{U}} \in \{-1, 1\}$; $p(t)$ is the transmitted monocycle shape, with energy $1/N_s$; T_f is the monocycle repetition time (frame length), and is related to the bit duration by $T_U = N_sT_f$; and $\{c_{i,k}\}_{k=0}^{N_s-1}$ is the spreading sequence, with $c_{i,k} \in \{-1, 1\}$. For such a DS-BPAM system, $\mathbf{W}_i(f_N)$ in (64) can be easily derived as

$$\mathbf{W}_i(f_N) = P(f_N)\sum_{k=0}^{N_s-1} c_{i,k}e^{j2\pi f_N kT_f}$$

where $P(f) \triangleq \mathcal{F}\{p(t)\}$. Different monocycle shapes are considered to satisfy FCC masks with the maximum transmitted power. Similarly to [99], we choose the 5th derivative of a Gaussian monocycle, so the received pulse can be modeled as the 6th derivative. In this case, we can write $P(f_N)$ as

$$P(f_N) = \frac{8\pi^3}{3\sqrt{1155N_s}}\tau_p^{13/2}f_N^6 e^{-\frac{\pi}{2}f_N^2\tau_p^2}$$

where τ_p is the monocycle duration parameter.

Concerning the NB propagation characteristics, we consider frequency-flat Rayleigh fading (i.e., $m = 1$). For the UWB propagation, we consider that the multipath fading channel in (58) is composed of L independent

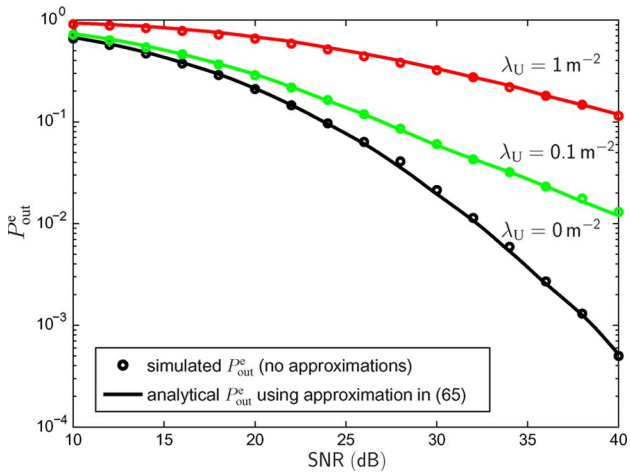

Fig. 11. ***P^e_{out} versus the SNR of the NB link for various spatial densities λ_U of the UWB interferers (NB link: BPSK, square $g(t)$ of duration $T_N = 1$ μs, $f_N = 5010$ GHz, $b_N = 2$, $\sigma_{N,dB} = 3$, frequency-flat Rayleigh fading, $p^* = 10^{-2}$, $r_0 = 1$ m; UWB interferers: DS-BPAM, $T_U = 0.8$ μs, $\tau_p = 0.192$ ns, INR $= 20$ dB, $N_s = 16$, $c_k^{ps} = (-1)^k$, $b_U = 2$, $\sigma_{U,dB} = 8$, frequency-selective Nakagami-m fading, $L = 8$, $\epsilon_p = 3$, $m_1 = 3$, $\epsilon_m = 4$).***

Nakagami-distributed paths having random delays and an exponential power dispersion profile [100], [101] given by

$$\Omega_q = \frac{e^{1/\epsilon_p} - 1}{1 - e^{-L/\epsilon_p}} e^{-q/\epsilon_p}, \qquad q = 1 \ldots L \tag{77}$$

where ϵ_p is a decay constant that controls the multipath dispersion. We also consider different Nakagami parameters for each path [101] according to

$$m_q = m_1 e^{-(q-1)/\epsilon_m}, \qquad q = 1 \ldots L \tag{78}$$

where ϵ_m controls the decay of the m-parameters.

The plots presented in this section are of semi-analytical nature. Specifically, we resort to a hybrid method where we employ the analytical expressions for P^e_{out}, and perform a Monte Carlo simulation of the stable RV A according to [102]. Nevertheless, we emphasize that the expressions derived in this paper completely eliminate the need for bit-level simulation, in order to obtain error performance results.

Fig. 11 quantifies the error performance of the BPSK NB link, subject to DS-BPAM UWB network interference and noise. For this purpose, we define the normalized SNR of the NB link as $\mathsf{SNR} = k_N^2 E_N / N_0$, and the normalized INR as $\mathsf{INR} = k_U^2 E_U / N_0$.[32] We conclude that the error performance of NB communication subject to UWB network interference deteriorates as λ_U or the INR increase, for a fixed SNR. This is expected because as the spatial density or transmitted energy of the UWB interferers increase, the aggregate interference at the NB victim receiver becomes stronger.

[32]Since E_N corresponds to the average transmitted symbol energy of the NB victim link, then $k_N^2 E_N$ can be interpreted as the average symbol energy measured 1 m away from the NB transmitter. An analogous interpretation applies to $k_U^2 E_U$.

VIII. CONCLUSION

In this paper, we presented a unifying framework for the characterization of network interference in wireless systems, where the interferers are scattered according to a spatial Poisson process. We first derived the characteristic function of the aggregate interference generated by a general set of active nodes. We then showed that when all the nodes in the plane are active, the aggregate interference amplitude follows a *symmetric stable* distribution, while the aggregate interference power follows a *skewed stable* distribution. These results are valid for arbitrary wireless propagation effects.

We further investigate four applications of the proposed model: 1) interference in cognitive radio networks; 2) interference in wireless packet networks; 3) spectrum of the aggregate RF emission of a wireless network; and 4) interference between UWB and NB systems. Our framework accounts for all the essential physical parameters that affect network interference, such as the type of wireless propagation effects, the type of transmission technology, the spatial density of interferers, and the transmitted power of the interferers. While we have explored some applications of the proposed framework, it is our hope that this paper will inspire other researchers to explore other applications. ■

APPENDIX I
DERIVATION OF (13)

Since $\mathbf{Q}_i$ is SS, we can write the characteristic function of each coordinate $Q_{i,n}$ as $\phi_0(t) \triangleq \phi_{\mathbf{Q}}(\mathbf{w})|_{|\mathbf{w}|=t}$. As a result

$$\begin{aligned}\phi_0(t) &= \phi_{Q_{i,n}}(t) \\ &= \mathbb{E}\{e^{\jmath t Q_{i,n}}\} \\ &= \mathbb{E}\{\cos(tQ_{i,n})\} + \jmath \underbrace{\mathbb{E}\{\sin(tQ_{i,n})\}}_{=0} \\ &= \mathbb{E}\{\cos(tQ_{i,n})\}.\end{aligned}$$

Using the elementary integral [103, Eq. 3.823], we can write

$$\int_0^\infty \frac{1 - \cos(zt)}{t^{\alpha+1}} dt = \frac{\Gamma(1-\alpha)\cos\left(\frac{\pi\alpha}{2}\right)}{\alpha} |z|^\alpha \tag{79}$$

for any real constants z and $0 < \alpha < 2$.[33] For $z = Q_{i,n}$ and taking expectations on both sides, we obtain

$$\int_0^\infty \frac{1-\phi_0(t)}{t^{\alpha+1}}\,dt = \frac{\Gamma(1-\alpha)\cos\left(\frac{\pi\alpha}{2}\right)}{\alpha}\,\mathbb{E}\left\{|Q_{i,n}|^\alpha\right\}. \quad (80)$$

Noting that $\Gamma(1-\alpha) = \Gamma(2-\alpha)/(1-\alpha)$ for $\alpha \neq 1$, we rewrite (80) as

$$\int_0^\infty \frac{1-\phi_0(t)}{t^{\alpha+1}}\,dt = \frac{C_\alpha^{-1}}{\alpha}\,\mathbb{E}\left\{|Q_{i,n}|^\alpha\right\}$$

where C_α is defined in (12). This is the result in (13), and the derivation is complete.

APPENDIX II
DERIVATION OF (19)

We start with the elementary integral [104, Eq. (4.11), p. 542]

$$\int_0^\infty \frac{1-e^{\jmath zt}}{t^{\alpha+1}}\,dt = \frac{\Gamma(1-\alpha)}{\alpha}|z|^\alpha\left[\cos\left(\frac{\pi\alpha}{2}\right) - \jmath\,\mathrm{sign}(z)\sin\left(\frac{\pi\alpha}{2}\right)\right]$$

[33]Note that (79) is still valid for $\alpha = 1$, provided that the right side is interpreted in the limiting sense of $\alpha \to 1$.

for any real constants z and $0 < \alpha < 1$. For $z = \mathrm{sign}(w)P_i$ and taking expectations on both sides, we obtain

$$\int_0^\infty \frac{1-\mathbb{E}\left\{e^{\jmath\,\mathrm{sign}(w)P_i t}\right\}}{t^{\alpha+1}}\,dt = \mathbb{E}\left\{P_i^\alpha\right\}\frac{\Gamma(1-\alpha)\cos\left(\frac{\pi\alpha}{2}\right)}{\alpha}\left[1-\jmath\,\mathrm{sign}(w)\tan\left(\frac{\pi\alpha}{2}\right)\right].$$

Noting that $\Gamma(1-\alpha) = \Gamma(2-\alpha)/(1-\alpha)$, we rewrite (81) as

$$\int_0^\infty \frac{1-\mathbb{E}\left\{e^{\jmath\,\mathrm{sign}(w)P_i t}\right\}}{t^{\alpha+1}}\,dt = \mathbb{E}\left\{P_i^\alpha\right\}\frac{C_\alpha^{-1}}{\alpha}\left[1-\jmath\,\mathrm{sign}(w)\tan\left(\frac{\pi\alpha}{2}\right)\right]$$

where C_α is defined in (12). This is the result in (19), and the derivation is complete.

Acknowledgment

The authors gratefully acknowledge helpful discussions with N. C. Beaulieu, M. Chiani, G. J. Foschini, L. J. Greenstein, R. A. Scholtz, and J. H. Winters. They would also like to thank A. Conti, D. Dardari, A. Giorgetti, Y. Shen, W. Suwansantisuk, and A. Zanella for their suggestions and careful readings of the manuscript.

REFERENCES

[1] A. J. Viterbi and I. M. Jacobs, "Advances in coding and modulation for noncoherent channels affected by fading, partial band, and multiple-access interference," in *Advances in Communication Systems: Theory and Applications*, vol. 4. New York: Academic, 1975, 279–308.

[2] I. M. I. Habbab, M. Kavehrad, and C. E. W. Sundberg, "ALOHA with capture over slow and fast fading radio channels with coding and diversity," *IEEE J. Sel. Areas Commun.*, vol. 7, pp. 79–88, Jan. 1989.

[3] K. Zhang and K. Pahlavan, "A new approach for the analysis of the slotted ALOHA local packet radio networks," in *Proc. IEEE Int. Conf. on Commun.*, Atlanta, GA, Apr. 1990, pp. 1231–1235.

[4] J. Linnartz, H. Goossen, R. Hekmat, K. Pahlavan, and K. Zhang, "Comment on slotted ALOHA radio networks with PSK modulation in Rayleigh fading channels," *Electron. Lett.*, vol. 26, pp. 593–595, Apr. 1990.

[5] N. C. Beaulieu and A. A. Abu-Dayya, "Bandwidth efficient QPSK in cochannel interference and fading," *IEEE Trans. Commun.*, vol. 43, no. 9, pp. 2464–2474, 1995.

[6] J. Cheng and N. C. Beaulieu, "Accurate DS-CDMA bit-error probability calculation in Rayleigh fading," *IEEE Trans. Wireless Commun.*, vol. 1, pp. 3–15, Jan. 2002.

[7] W. Feller, *An Introduction to Probability Theory and Its Applications*, vol. 2. New York: Wiley, 1971.

[8] S. A. Kassam, *Signal Detection in Non-Gaussian Noise*. New York: Springer, 1988.

[9] E. J. Wegman, S. C. Schwartz, and J. B. Thomas, *Topics in Non-Gaussian Signal Processing*. New York: Springer, 1989.

[10] M. Chiani, "Analytical distribution of linearly modulated cochannel interferers," *IEEE Trans. Commun.*, vol. 45, pp. 73–79, Jan. 1997.

[11] A. Giorgetti and M. Chiani, "Influence of fading on the Gaussian approximation for BPSK and QPSK with asynchronous cochannel interference," *IEEE Trans. Wireless Commun.*, vol. 4, pp. 384–389, 2005.

[12] B. Hu and N. C. Beaulieu, "Accurate evaluation of multiple access performance in TH-PPM and TH-BPSK UWB systems," *IEEE Trans. Commun.*, vol. 52, pp. 1758–1766, Oct. 2004.

[13] B. Hu and N. C. Beaulieu, "Exact bit error rate of TH-PPM UWB systems in the presence of multiple access interference," *IEEE Commun. Lett.*, vol. 7, pp. 572–574, Dec. 2003.

[14] D. Middleton, "Statistical-physical models of electromagnetic interference," *IEEE Trans. Electromagn. Compat.*, vol. 19, pp. 106–127, Aug. 1977.

[15] D. Middleton, "Non-Gaussian noise models in signal processing for telecommunications: New methods and results for class A and class B noise models," *IEEE Trans. Inf. Theory*, vol. 45, no. 4, pp. 1129–1149, May 1999.

[16] G. V. Trunk and S. F. George, "Detection of targets in non-Gaussian sea clutter," *IEEE Trans. Aerosp. Electron. Syst.*, vol. 6, no. 5, pp. 620–628, Sep. 1970.

[17] G. V. Trunk, "Further results on the detection of targets in non-Gaussian sea clutter," *IEEE Trans. Aerosp. Electron. Syst.*, vol. 7, pp. 553–556, May 1971.

[18] M. Shao and C. Nikias, "Signal processing with fractional lower order moments: Stable processes and their applications," *Proc. IEEE*, vol. 81, no. 7, pp. 986–1010, 1993.

[19] C. L. Nikias and M. Shao, *Signal Processing With Alpha-Stable Distributions and*

Applications. New York: Wiley-Interscience, 1995.

[20] J. Silvester and L. Kleinrock, "On the capacity of multihop slotted ALOHA networks with regular structure," *IEEE Trans. Commun.*, vol. 31, pp. 974–982, Aug. 1983.

[21] R. Mathar and J. Mattfeldt, "On the distribution of cumulated interference power in Rayleigh fading channels," *Wireless Netw.*, vol. 1, pp. 31–36, Feb. 1995.

[22] G. Ferrari and O. K. Tonguz, "Minimum number of neighbors for fully connected uniform ad hoc wireless networks," in *Proc. IEEE Int. Conf. Commun.*, Jun. 2004, vol. 7, pp. 4331–4335.

[23] X. Liu and M. Haenggi, "The impact of the topology on the throughput of interference-limited sensor networks with rayleigh fading," in *Proc. IEEE Conf. on Sensor and Ad Hoc Commun. and Networks*, Sep. 2005, pp. 317–327.

[24] J. Kingman, *Poisson Processes*. Oxford, U.K.: Oxford Univ. Press, 1993.

[25] J. A. McFadden, "The entropy of a point process," *J. Soc. Ind. Appl. Math.*, vol. 13, no. 4, pp. 988–994, Dec. 1965.

[26] J. Orriss and S. K. Barton, "Probability distributions for the number of radio transceivers which can communicate with one another," *IEEE Trans. Commun.*, vol. 51, pp. 676–681, Apr. 2003.

[27] A. Conti, D. Dardari, and R. Verdone, "Collaborative signal processing for energy-efficient self-organizing wireless sensor network," in *Proc. Int. Workshop on Wireless Ad Hoc Networks*, May/Jun. 2004, pp. 99–104.

[28] C. Bettstetter and C. Hartmann, "Connectivity of wireless multihop networks in a shadow fading environment," *Wireless Netw.*, vol. 11, no. 5, pp. 571–579, Sep. 2005.

[29] D. Miorandi and E. Altman, "Coverage and connectivity of ad hoc networks in presence of channel randomness," in *Proc. IEEE Conf. on Computer Commun.*, Mar. 2005, vol. 1, pp. 491–502.

[30] T. Q. S. Quek, D. Dardari, and M. Z. Win, "Energy efficiency of dense wireless sensor networks: To cooperate or not to cooperate," *IEEE J. Sel. Areas Commun.*, vol. 25, pp. 459–470, Feb. 2007.

[31] E. Salbaroli and A. Zanella, "A connectivity model for the analysis of a wireless ad hoc network in a circular area," in *Proc. IEEE Int. Conf. on Commun.*, Jun. 2007, pp. 4937–4942.

[32] E. Salbaroli and A. Zanella, "Interference characterization in a finite Poisson field of nodes with shadowing," in *Proc. IEEE Int. Symp. on Personal, Indoor and Mobile Radio Commun.*, France, Sep. 2008, pp. 1–6.

[33] H. Takagi and L. Kleinrock, "Optimal transmission ranges for randomly distributed packet radio terminals," *IEEE Trans. Commun.*, vol. COM-32, pp. 246–257, Mar. 1984.

[34] T.-C. Hou and V. Li, "Transmission range control in multihop packet radio networks," *IEEE Trans. Commun.*, vol. COM-34, pp. 38–44, Jan. 1986.

[35] E. S. Sousa and J. A. Silvester, "Optimum transmission ranges in a direct-sequence spread-spectrum multihop packet radio network," *IEEE J. Sel. Areas Commun.*, vol. 8, pp. 762–771, Jun. 1990.

[36] F. Baccelli, B. Blaszczyszyn, and P. Muhlethaler, "A spatial reuse ALOHA MAC protocol for multihop wireless mobile networks," Institut National de Recherche en Informatique et en Automatique (INRIA), Rocquencourt, Le Chesnay Cedex, France, Tech. Rep. 4955, Oct. 2003.

[37] M. Haenggi, "Outage and throughput bounds for stochastic wireless networks," in *Proc. IEEE Int. Symp. on Inform. Theory*, Sep. 2005, pp. 2070–2074.

[38] J. Venkataraman, M. Haenggi, and O. Collins, "Shot noise models for outage and throughput analyses in wireless ad hoc networks," in *Proc. Military Commun. Conf.*, Washington, D.C., Oct. 2006, pp. 1–7.

[39] E. Sousa, "Performance of a spread spectrum packet radio network link in a Poisson field of interferers," *IEEE Trans. Inf. Theory*, vol. 38, no. 6, pp. 1743–1754, 1992.

[40] S. Ambike, J. Ilow, and D. Hatzinakos, "Detection for binary transmission in a mixture of gaussian noise and impulsive noise modeled as an alpha-stable process," *IEEE Signal Process. Lett.*, vol. 1, no. 3, pp. 55–57, 1994.

[41] G. Tsihrintzis and C. Nikias, "Performance of optimum and suboptimum receivers in the presence of impulsive noise modeled as an alpha-stable process," *IEEE Trans. Commun.*, vol. 43, no. 234, pp. 904–914, 1995.

[42] J. Ilow, D. Hatzinakos, and A. Venetsanopoulos, "Performance of FH SS radio networks with interference modeled as a mixture of Gaussian and alpha-stable noise," *IEEE Trans. Commun.*, vol. 46, no. 4, pp. 509–520, 1998.

[43] S. Govindasamy, F. Antic, D. Bliss, and D. Staelin, "The performance of linear multiple-antenna receivers with interferers distributed on a plane," in *Proc. IEEE Workshop on Signal Process. Advances in Wireless Commun.*, 2005, pp. 880–884.

[44] A. Rabbachin, T. Q. Quek, P. C. Pinto, I. Oppermann, and M. Z. Win, "UWB energy detection in the presence of multiple narrowband interferers," in *Proc. IEEE Int. Conf. Ultra-Wideband (ICUWB)*, Singapore, Sep. 2007, pp. 857–862.

[45] A. Rabbachin, T. Q. Quek, P. C. Pinto, I. Oppermann, and M. Z. Win, "Effect of aggregate narrowband interference on the UWB autocorrelation receiver," in *Proc. IEEE Int. Conf. Ultra-Wideband (ICUWB)*, Hannover, Germany, Sep. 2008.

[46] P. C. Pinto, J. Barros, and M. Z. Win, "Physical-layer security in stochastic wireless networks," in *Proc. IEEE Int. Conf. Commun. Syst.*, Guangzhou, China, Nov. 2008, pp. 974–979.

[47] D. P. Bertsekas and J. N. Tsitsiklis, *Introduction to Probability*. Nashua, NH: Athena Scientific, 2008.

[48] A. Goldsmith, *Wireless Communications*. Cambridge, U.K.: Cambridge Univ. Press, 2005.

[49] G. L. Stüber, *Principles of Mobile Communication*. New York: Springer, 2000.

[50] L. J. Greenstein, V. Erceg, Y. S. Yeh, and M. V. Clark, "A new path-gain/delay-spread propagation model for digital cellular channels," *IEEE Trans. Veh. Technol.*, vol. 46, pp. 477–485, May 1997.

[51] A. Conti, M. Z. Win, and M. Chiani, "Invertible bounds for *M*-QAM in fading channels," *IEEE Trans. Wireless Commun.*, vol. 4, pp. 1994–2000, Sep. 2005.

[52] A. Conti, M. Z. Win, and M. Chiani, "On the inverse symbol error probability for diversity reception," *IEEE Trans. Commun.*, vol. 51, pp. 753–756, May 2003.

[53] A. Conti, M. Z. Win, M. Chiani, and J. H. Winters, "Bit error outage for diversity reception in shadowing environment," *IEEE Commun. Lett.*, vol. 7, pp. 15–17, Jan. 2003.

[54] A. A. Abu-Dayya and N. C. Beaulieu, "Micro- and macrodiversity NCFSK (DPSK) on shadowed Nakagami-fading channels," *IEEE Trans. Commun.*, vol. 42, pp. 2693–2702, Sep. 1994.

[55] P. C. Pinto and M. Z. Win, "Communication in a Poisson field of interferers—Part I: Interference distribution and error probability," *IEEE Trans. Wireless Commun.*, 2008, to appear.

[56] P. C. Pinto, A. Giorgetti, and M. Z. Win, "A stochastic geometry approach to coexistence in heterogeneous wireless networks," *IEEE J. Sel. Areas Commun.*, 2008, submitted for publication.

[57] G. Samoradnitsky and M. Taqqu, *Stable Non-Gaussian Random Processes*. London, U.K.: Chapman and Hall, 1994.

[58] M. McHenry, "NSF Spectrum Occupancy Measurements Project Summary," Shared Spectrum Company, 2005.

[59] J. I. Mitola and G. Q. J. Maguire, "Cognitive radio: Making software radios more personal," *IEEE Pers. Commun.*, vol. 6, pp. 13–18, Aug. 1999.

[60] S. E. Heath, "Applications of the Poisson model to wireless telephony and to cosmology," Ph.D. dissertation, Rutgers Univ., New Brunswick, NJ, Mar. 2004.

[61] J. Abate and W. Whitt, "The Fourier-series method for inverting transforms of probability distributions," *Queueing Syst.*, vol. 10, pp. 5–88, 1992.

[62] M. Abramowitz and I. A. Stegun, *Handbook of Mathematical Functions*. New York: Dover, 1970.

[63] P. C. Pinto and M. Z. Win, "Throughput in wireless packet networks: A unifying framework," Massachusetts Institute of Technology, Laboratory for Information & Decision Systems (LIDS) Internal Report, Feb. 2009.

[64] N. B. Mehta, J. Wu, A. F. Molisch, and J. Zhang, "Approximating a sum of random variables with a lognormal," *IEEE Trans. Wireless Commun.*, vol. 6, no. 7, pp. 2690–2699, 2007.

[65] P. C. Pinto and M. Z. Win, "A unified analysis of connectivity and throughput in packet radio networks," in *Proc. Military Commun. Conf.*, San Diego, CA, Nov. 2008, pp. 1–7.

[66] N. Abramson, "The throughput of packet broadcasting channels," *IEEE Trans. Commun.*, vol. COM-25, pp. 117–128, Jan. 1977.

[67] P. C. Pinto and M. Z. Win, "Communication in a Poisson field of interferers—Part II: Channel capacity and interference spectrum," *IEEE Trans. Wireless Commun.*, 2008, to appear.

[68] P. C. Pinto and M. Z. Win, "Spectral characterization of wireless networks," *IEEE Wireless Commun. Mag. (Special Issue on Wireless Sensor Networking)*, vol. 14, pp. 27–31, Dec. 2007.

[69] P. A. Bello, "Characterization of randomly time-variant linear channels," *IEEE Trans. Commun. Syst.*, vol. CS-11, pp. 360–393, Dec. 1963.

[70] J. D. Parsons, *The Mobile Radio Propagation Channel*, 2nd ed. New York: Wiley, 2000.

[71] R. Steele, *Mobile Radio Communications*, 2nd ed. New York: IEEE Press, 1999.

[72] J. Proakis, *Digital Communications*, 5th ed. McGraw-Hill, 2008.

[73] A. F. Molisch, *Wireless Communications*, 1st ed. Piscataway, NJ: IEEE Press/Wiley, 2005.

[74] P. C. Pinto and M. Z. Win, "Spectral outage due to cumulative interference in a Poisson field of nodes," in *Proc. IEEE Global Telecomm. Conf.*, San Francisco, CA, Nov. 2006, pp. 1–6.

[75] P. C. Pinto and M. Z. Win, "Design of covert military networks: A spectral outage-based approach," in *Proc. Military Commun. Conf.*, Washington, DC, Oct. 2006, pp. 1–6.

[76] W. A. Gardner, *Introduction to Random Processes With Applications to Signals and Systems*, 2nd ed. New York: McGraw-Hill, 1990.

[77] A. Papoulis and S. U. Pillai, *Probability, Random Variables and Stochastic Processes*, 4th ed. New York: McGraw-Hill, 2002.

[78] M. K. Simon, S. M. Hinedi, and W. C. Lindsey, *Digital Communication Techniques: Signal Design and Detection*, 1st ed. Englewood Cliffs, NJ: Prentice-Hall, 1994.

[79] M. Z. Win, "On the power spectral density of digital pulse streams generated by *M*-ary cyclostationary sequences in the presence of stationary timing jitter," *IEEE Trans. Commun.*, vol. 46, pp. 1135–1145, Sep. 1998.

[80] M. Z. Win, "A unified spectral analysis of generalized time-hopping spread-spectrum signals in the presence of timing jitter," *IEEE J. Sel. Areas Commun.*, vol. 20, pp. 1664–1676, Dec. 2002.

[81] M. Z. Win and R. A. Scholtz, "Impulse radio: How it works," *IEEE Commun. Lett.*, vol. 2, pp. 36–38, Feb. 1998.

[82] M. Z. Win and R. A. Scholtz, "Ultra-wide bandwidth time-hopping spread-spectrum impulse radio for wireless multiple-access communications," *IEEE Trans. Commun.*, vol. 48, pp. 679–691, Apr. 2000.

[83] M. Z. Win and R. A. Scholtz, "Characterization of ultra-wide bandwidth wireless indoor communications channel: A communication theoretic view," *IEEE J. Sel. Areas Commun.*, vol. 20, pp. 1613–1627, Dec. 2002.

[84] T. Q. S. Quek and M. Z. Win, "Analysis of UWB transmitted-reference communication systems in dense multipath channels," *IEEE J. Sel. Areas Commun.*, vol. 23, pp. 1863–1874, Sep. 2005.

[85] W. Suwansantisuk, M. Z. Win, and L. A. Shepp, "On the performance of wide-bandwidth signal acquisition in dense multipath channels," *IEEE Trans. Veh. Technol. (Special Section on Ultra-Wideband Wireless Communications—A New Horizon)*, vol. 54, pp. 1584–1594, Sep. 2005.

[86] S. Haykin, "Cognitive radio: Brain-empowered wireless communications," *IEEE J. Sel. Areas Commun.*, vol. 23, pp. 201–220, Feb. 2005.

[87] M. Chiani, A. Giorgetti, and G. Liva, "Ultra wide bandwidth communications towards cognitive radio," in *Proc. EMC Eur. Workshop 2005—Electromagn. Comp. Wireless Syst.*, Rome, Italy, Sep. 2005, pp. 114–117.

[88] A. Giorgetti, M. Chiani, and D. Dardari, "Coexistence issues in cognitive radios based on ultra-wide bandwidth systems," in *Proc. IEEE Int. Conf. on Cognitive Radio Oriented Wireless Networks and Commun.*, Mykonos, Greece, Jun. 2006.

[89] P. C. Pinto, C.-C. Chong, A. Giorgetti, M. Chiani, and M. Z. Win, "Narrowband communication in a Poisson field of ultrawideband interferers," in *Proc. of IEEE Int. Conf. Ultra-Wideband (ICUWB)*, Waltham, MA, Sept. 2006, pp. 387–392.

[90] M. Z. Win, P. C. Pinto, A. Giorgetti, M. Chiani, and L. A. Shepp, "Error performance of ultrawideband systems in a Poisson field of narrowband interferers," in *Proc. IEEE Int. Symp. Spread Spectrum Tech. Applicat.*, Manaus, Brazil, Aug. 2006, pp. 410–416.

[91] T. M. Cover and J. A. Thomas, *Elements of Information Theory*, 2nd ed. New York: Wiley-Interscience, 2006.

[92] J. W. Craig, "A new, simple and exact result for calculating the probability of error for two-dimensional signal constellations," in *Proc. Military Commun. Conf.*, Boston, MA, 1991, pp. 25.5.1–25.5.5.

[93] X. Dong, N. C. Beaulieu, and P. H. Wittke, "Error probabilities of two-dimensional *M*-ary signaling in fading," *IEEE Trans. Commun.*, vol. 47, pp. 352–355, Mar. 1999.

[94] M. Z. Win and J. H. Winters, "Virtual branch analysis of symbol error probability for hybrid selection/maximal-ratio combining in Rayleigh fading," *IEEE Trans. Commun.*, vol. 49, pp. 1926–1934, Nov. 2001.

[95] M. K. Simon and M.-S. Alouini, *Digital Communication Over Fading Channels*, 2nd ed. New York: Wiley, 2004, 10158.

[96] W. M. Gifford, M. Z. Win, and M. Chiani, "Diversity with practical channel estimation," *IEEE Trans. Wireless Commun.*, vol. 4, pp. 1935–1947, Jul. 2005.

[97] M. Z. Win, G. Chrisikos, and J. H. Winters, "MRC performance for *M*-ary modulation in arbitrarily correlated Nakagami fading channels," *IEEE Commun. Lett.*, vol. 4, pp. 301–303, Oct. 2000.

[98] W. M. Gifford, M. Z. Win, and M. Chiani, "Antenna subset diversity with non-ideal channel estimation," *IEEE Trans. Wireless Commun.*, vol. 7, no. 5, pp. 1527–1539, May 2008.

[99] A. Giorgetti and D. Dardari, "The impact of OFDM interference on TH-PPM/BPAM transmission systems," in *Proc. IEEE Semiannual Veh. Technol. Conf.*, vol. 2, 2005, pp. 1037–1042.

[100] D. Cassioli, M. Z. Win, and A. F. Molisch, "The ultra-wide bandwidth indoor channel: From statistical model to simulations," *IEEE J. Sel. Areas Commun.*, vol. 20, pp. 1247–1257, Aug. 2002.

[101] A. Giorgetti, M. Chiani, and M. Z. Win, "The effect of narrowband interference on wideband wireless communication systems," *IEEE Trans. Commun.*, vol. 53, pp. 2139–2149, Dec. 2005.

[102] J. Chambers, C. Mallows, and B. Stuck, "A method for simulating stable random variables," *J. Amer. Statist. Assoc.*, vol. 71, pp. 340–344, 1976.

[103] I. S. Gradshteyn and I. M. Ryzhik, *Tables of Integrals, Series, and Products*, 7th ed. San Diego, CA: Academic, 2007.

[104] W. Feller, *An Introduction to Probability Theory and Its Applications*, vol. 2. New York: Wiley, 1966.

ABOUT THE AUTHORS

Moe Z. Win (Fellow, IEEE) received both the Ph.D. in Electrical Engineering and M.S. in Applied Mathematics as a Presidential Fellow at the University of Southern California (USC) in 1998. He received an M.S. in Electrical Engineering from USC in 1989, and a B.S. (*magna cum laude*) in Electrical Engineering from Texas A&M University in 1987.

Dr. Win is an Associate Professor at the Massachusetts Institute of Technology (MIT). Prior to joining MIT, he was at AT&T Research Laboratories for five years and at the Jet Propulsion Laboratory for seven years. His research encompasses developing fundamental theory, designing algorithms, and conducting experimentation for a broad range of real-world problems. His current research topics include location-aware networks, time-varying channels, multiple antenna systems, ultra-wide bandwidth systems, optical transmission systems, and space communications systems.

Professor Win is an IEEE Distinguished Lecturer and an elected Fellow of the IEEE cited for "contributions to wideband wireless transmission." He was honored with the IEEE Eric E. Sumner Award (2006), an IEEE Technical Field Award for "pioneering contributions to ultra-wide band communications science and technology." Together with students and colleagues, his papers have received several awards including the IEEE Communications Society's Guglielmo Marconi Best Paper Award (2008) and the IEEE Antennas and Propagation Society's Sergei A. Schelkunoff Transactions Prize Paper Award (2003). His other recognitions include the Laurea Honoris Causa from the University of Ferrara, Italy (2008), the Technical Recognition Award of the IEEE ComSoc Radio Communications Committee (2008), Wireless Educator of the Year Award (2007), the Fulbright Foundation Senior Scholar Lecturing and Research Fellowship (2004), the U.S. Presidential Early Career Award for Scientists and Engineers (2004), the AIAA Young Aerospace Engineer of the Year (2004), and the Office of Naval Research Young Investigator Award (2003).

Professor Win has been actively involved in organizing and chairing a number of international conferences. He served as the Technical Program Chair for the IEEE Wireless Communications and Networking Conference in 2009, the IEEE Conference on Ultra Wideband in 2006, the IEEE Communication Theory Symposia of ICC-2004 and Globecom-2000, and the IEEE Conference on Ultra Wideband Systems and Technologies in 2002; Technical Program Vice-Chair for the IEEE International Conference on Communications in 2002; and the Tutorial Chair for ICC-2009 and the IEEE Semiannual International Vehicular Technology Conference in Fall 2001. He was the chair (2004–2006) and secretary (2002–2004) for the Radio Communications Committee of the IEEE Communications Society. Dr. Win is currently an Editor for IEEE TRANSACTIONS ON WIRELESS COMMUNICATIONS. He served as Area Editor for *Modulation and Signal Design* (2003-2006), Editor for *Wideband Wireless and Diversity* (2003–2006), and Editor for *Equalization and Diversity* (1998–2003), all for the IEEE TRANSACTIONS ON COMMUNICATIONS. He was Guest-Editor for the IEEE JOURNAL ON SELECTED AREAS IN COMMUNICATIONS (Special Issue on Ultra-Wideband Radio in Multiaccess Wireless Communications) in 2002.

Pedro C. Pinto (Student Member, IEEE) received the Licenciatura degree with highest honors in Electrical and Computer Engineering from the Oporto University, Portugal, in 2003. He received the M.S. degree in Electrical Engineering and Computer Science from the Massachusetts Institute of Technology (MIT) in 2006. Since 2004, he has been with the MIT Laboratory for Information and Decision Systems (LIDS), where he is now a Ph.D. candidate. His main research interests are in wireless communications and signal processing. He was the recipient of the MIT Claude E. Shannon Fellowship in 2007, the Best Student Paper Award at the IEEE International Conference on Ultra-Wideband in 2006, and the Infineon Technologies Award in 2003.

Lawrence A. Shepp received the B.S. degree in applied mathematics from the Polytechnic Institute of Brooklyn in 1958, and the M.A. and Ph.D. degrees in mathematics from Princeton University in 1960 and 1961, respectively.

He joined the Mathematics Research Center of AT&T Bell Laboratories in 1962 and became a Distinguished Member of Technical Staff at Bell Laboratories in 1986. He was a Professor of Statistics and Operations Research at Columbia University from 1996 to 1997. In 1997, he joined the Department of Statistics at Rutgers University, where he is Board of Governor's Professor. During his career at AT&T, he held various joint appointments: he was a Professor of Radiology at Columbia University from 1973 to 1996, a Mathematician in Radiology Service at the Columbia Presbyterian Hospital from 1974 to 1996, and a Professor of Statistics (1/4 time) at Stanford University from 1978 to 1992. He was a member of the Scientific Boards of American Science and Engineering Inc. from 1974 to 1975 and of Resonex Inc. from 1983 to 1984. Dr. Shepp spent extended visiting periods at many places including the Mittag-Leffler Institute, MIT, the University of New South Wales, the Australian National University, and Simon Bolivar University in Caracas. He was an exchange scholar at the Steklov Institute in Moscow for 6 months in 1966. He has a permanent visiting position at University of Coral Gables and also at Stanford University. His current research interests include functional magnetic resonance imaging, tomography, wireless telephony, cosmology, and the mathematics of finance.

Prof. Shepp has made fundamental contributions to CAT scanning, emission tomography, probability theory (random covering, Gaussian processes, connectedness of random graphs), mathematical finance and economics. He is a Co-Editor for the *Wiley International Journal of Imaging Systems and Technology* and was an Associate Editor for *Journal of Computer Assisted Tomography* from 1977 to 1992. He was elected to the National Academy of Science, the Institute of Medicine, the Academy of Arts and Science, and a Fellow of the Institute of Mathematical Statistics. He was the winner of the William Lowell Putnam Intercollegiate Mathematics Competition in 1958, the Paul Levy Prize in 1966, and he received an IEEE Distinguished Scientist Award in 1979.